Numerical Simulation of Snow Avalanche Impact on Structures

T. E. Lang and R. L. Brown

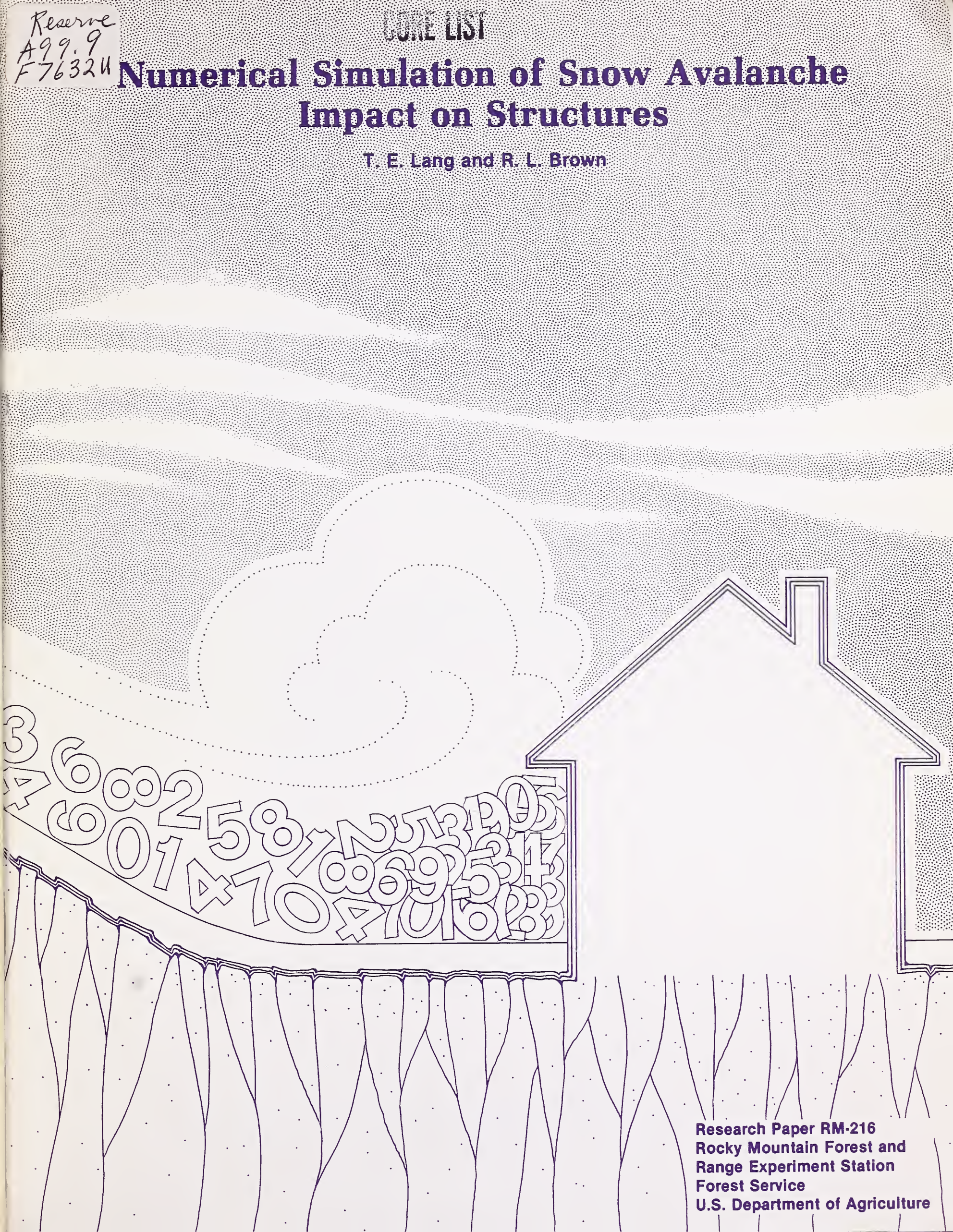

Research Paper RM-216
Rocky Mountain Forest and
Range Experiment Station
Forest Service
U.S. Department of Agriculture

Abstract

A computer model to predict snow avalanche impact on rigid wall structures is developed based on hydrodynamic equations for viscous flow, and admitting a frictional slip-plane lower boundary. Slope normal and vertical wall configurations which extend higher than the height of avalanche flow are evaluated for normal and shear force and overturning moment from avalanche impact. Impact forces and moment time depend upon avalanche leading edge shape.

USDA Forest Service
Research Paper RM-216

June 1980

Numerical Simulation of Snow Avalanche Impact on Structures[1]

T. E. Lang, Professor
Montana State University

and

R. L. Brown, Professor
Montana State University

[1]*Research was conducted under Cooperative Agreement 16-627CA between Montana State University and the USDA Forest Service, Rocky Mountain Forest and Range Experiment Station. Headquarters is at Fort Collins in cooperation with Colorado State University.*

Contents

Numerical Simulation of Snow Avalanche Impact on Structures

T. E. Lang and R. L. Brown

Management Implications

Power transmission line towers and bases, avalanche sheds, flow diversion barriers, and energy dissipative structures of various shapes are types of structures subject to snow avalanche flow and impact. Design of this type of structure has developed largely from experience and includes large factors of safety, which boost material and labor costs. Little engineering information is available to aid in establishing expected forces and stresses, particularly in situations involving snow impact.

This paper presents results from two analyses of structures impacted by avalanches at various speeds. Forces on the structures are presented in graphical form, so that design specialists may refer to these data to estimate forces and pressures for structures that correspond to those treated in the report.

The computer program developed to obtain the data described above is a general-purpose program available for use by persons involved in structural design. Structures of many different shapes may be input and subjected to snow avalanches of different speeds and depths. Output from the code are contact pressures and forces, flow profiles, and flow velocities of the snow as it impacts and flows around the structure. Thus, an impact becomes a pictorial display of the processes going on.

The numerical approach to representing avalanche flow and impact described in this report is a new development in the methods of dealing with the complex problems of snow avalanche mechanics. Use of the program by others is encouraged so that updates and changes can be made based upon user needs.

Introduction

When snow avalanches impact structures, large forces and pressures are set up that warrant consideration in structural design. Only limited data exist on the forces and pressures that can be expected from avalanches of different speeds and depths of flow. Data are from either actual physical observations of post-avalanche impacted structures, or from planned experiments over limited ranges of the primary parameters of speed-at-impact and flow depth.

Basic contributions to knowledge of snow impact were made by Voellmy (1964), who evaluated evidence from avalanches in Austria. He concluded that pressures in the range of 10 to 20 t/m² were necessary to account for the damage noted, and that this pressure range is attributable to the solid core of flowing snow, and not to the airborne component. For calculation of impact pressure, Voellmy proposed a version of the dynamic pressure equation with pressure proportional to the square of the flow velocity (or kinetic energy).

Furukawa (1957) reported results of releasing snow blocks to slide down a slope and impact a wall. Average pressure of impact was measured and correlated to other parameters by the equation

$$p = 3.5\left(1.35v^2 \frac{\varrho^{1.5}}{g}\right)^{0.45}$$

applicable in the range of densities $150<\varrho<550$ kg/m³ and impact velocity $5<v<20$ m/s. The time constant of the recording oscillograph of these experiments is 0.01 s, so that rapid variations in the loading are smooth. Pressures computed by Furukawa's equation fall into the same range as reported by Voellmy.

Saito et al. (1963) reported the results of experiments made on various avalanche control structures. Avalanche impact forces on posts set up in the avalanche path were measured. Maximum pressure was 30 t/m² with a range downward to an average of around 20 t/m². No information is given on depth of flow, nor on the nominal density of the impacting snow.

Salm (1964) presented results similar to those of Furukawa, except that force-recording equipment had a shorter time constant, so that millisecond duration pulses were detected. For snow blocks impacting at velocities of 11 to 13 m/s, average pressures were obtained in the range 15 to 20 t/m² for impact onto an elastically soft wall. Maximum pressures of load pulses of several milliseconds duration were recorded and found to be two to five times larger than average pressures reported above.

Perhaps the most complete set of data on avalanche impact is reported by Schaerer (1973) based upon a number of avalanche measurements made at Rodgers Pass, British Columbia, Canada.

Pressure gages mounted on posts in avalanche paths were used to monitor average impact pressure. Measurements also were made of depth of flow, nominal density of the snow debris and average avalanche speed. Based upon a dynamic pressure equation, Schaerer compared computed and measured pressures. Average pressures ranged from 3 to 26 t/m² for velocity variations from 15 to 53 m/s and flow depths between 1.5 and 1.8 m as evidenced from snow deposits on trees and side walls of the flow channels.

Additional evidence is reported by Mears (1975) based upon analysis of damaged trees in the path of an avalanche in Colorado. For flow speeds in the range of 18 m/s, loading was estimated at 8 to 10 t/m² for a flow height of 1.1 m and snow density of 300 kg/m³.

All of the above results tend to indicate average dynamic pressures up to 30 t/m² for flow velocities up to 40 m/s; although incomplete data reporting tends to prevent conclusive ranging. Shimuzu et al. (1973) reported different results based upon measurements of three avalanches in Kurobe Canyon, Japan. Indications from the discussion in this report are that the avalanches were "high speed;" however, no information was presented on the actual range of velocities of the avalanches. Pressures were reported from 32 to 134 t/m² depending upon type of recording system, and a maximum pressure of 210 t/m² is mentioned without elaboration or explanation. Lacking information on recording system response and velocities of the flows, it is possible to attribute these high pressures to either high impact velocity, or to reporting of maximum pressures of load pulses rather than of pressures averaged over 10 to 100 ms or more, as is done by Salm (1964) and Schaerer (1973).

Having an indication of the nature of the force (distribution in time) of typical avalanche impact, the possibility of computer simulation of the phenomenon was investigated.

This report summarizes new methodology for predicting impact of snow avalanches on structures. The approach involves computer modeling of the flow and impact using an iterative solution of the Navier-Stokes equations of motion for viscous, Newtonian fluid flow. Time and spatial advance of the fluid through the finite difference grid of the flow domain is carried out by iterative refinement of the momentum and mass distributions consistent with the governing equations. Original reporting of a computer algorithm for two-dimensional flow in either a closed or free-surface domain is by Hirt et al. (1975). Modification of this general purpose code to the specific modeling of avalanche flow is reported by Lang et al. (1979), which includes considerable detail on the characteristics and application of the code to avalanche flow problems. This report further modifies this code to facilitate calculation of pressure and force distributions on rigid structures subjected to avalanche impact. Computer simulation data are compared with existing physical information to evaluate its accuracy. Physical properties assumed for snow in the computer model are nominal properties that have been determined to be representative for avalanche runout prediction (Lang et al. 1979).

Computer simulation could be used to develop design criteria for structures without having to accumulate physical data from random avalanches.

Governing Equations and Flow Parameters

The flow characteristics of a possible airborne or snow-dust component of an avalanche must be distinguished from the flow of the denser or core component. Our consideration is directed to the core component, which has a typical velocity range of 20 to 50 m/s. Whether or not the core material behaves the same when surrounded by an airborne component is unknown. For snow having large viscosity, the flow is assumed to be incompressible, which is a conservative approximation when considering pressures and forces of impact upon obstacles.

The numerical analysis of snow avalanche impact is carried out for a "typical" cross-section of the flow, so that it is sufficient to consider two-dimensional forms of the governing equations. For an incompressible, viscous fluid, the equations of motion are the Navier-Stokes equations:

$$\frac{du}{dt} = X - \frac{1}{\varrho}\frac{\partial \varrho}{\partial x} + \nu\left(\frac{\partial^2 u}{\partial x^2} + \frac{\partial^2 u}{\partial y^2}\right)$$
$$\frac{dv}{dt} = Y - \frac{1}{\varrho}\frac{\partial p}{\partial y} + \nu\left(\frac{\partial^2 v}{\partial x^2} + \frac{\partial^2 v}{\partial y^2}\right) \qquad [1]$$

where

u,v = components of velocity (m/s)
t = time (s)
X,Y = components of of body force per unit of density (m²/s²)
ϱ = fluid density kg/m³
p = fluid pressure (Pa)
ν = kinematic viscosity (m²/s)
x,y = rectangular Cartesian coordinates (m)

and

$$\frac{d}{dt} = \frac{\partial}{\partial t} + u\frac{\partial}{\partial x} + v\frac{\partial}{\partial y}$$

Equation [1] is not sufficient to solve for the pressure, p, and two components of velocity, u and v. The additional equation needed is the mass continuity equation, which in two dimensions for either homogeneous or heterogenous incompressible flow takes the form

$$\frac{\partial u}{\partial x} + \frac{\partial v}{\partial y} = 0 \qquad [2]$$

This completes the number of equations needed to solve for the unknowns of the problem.

The stresses acting upon a fluid element are:

$$\tau_{xx} = -p + 2\mu\frac{\partial u}{\partial x}$$

$$\tau_{yy} = -p + 2\mu\frac{\partial v}{\partial y} \qquad [3]$$

$$\tau_{xy} = \mu\frac{\partial v}{\partial x} + \frac{\partial u}{\partial y}$$

where μ is the dynamic viscosity, which is related to the kinematic viscosity by $\nu = \mu/\varrho$. The pressure, p, is assumed to be compressional, and hence a negative contribution to stress. Equation [3] is needed to compute the forces that develop on the impacted obstacle as a result of fluid contact.

Finite difference versions of equations [1] and [2] are actually used in computer code AVALNCH (Lang et al. 1979) to simulate avalanche flow and impact. The code is written so that variable kinematic viscosity and surface friction coefficients can be used to represent the flow. Flow down a slope is simulated by assigning gravity components to the body force intensities, X and Y, of equation [1]. Actual computed parameter values from the code are normalized by material density, so that computed pressure is actually in units p/ϱ (m^2/s^2), stress is τ_{xx}/ϱ (m^2/s^2), and total impact force is F_x/ϱ (m^4/s^2). The finite difference grid that represents the flow domain plus a one-cell boundary layer is shown in figure 1.

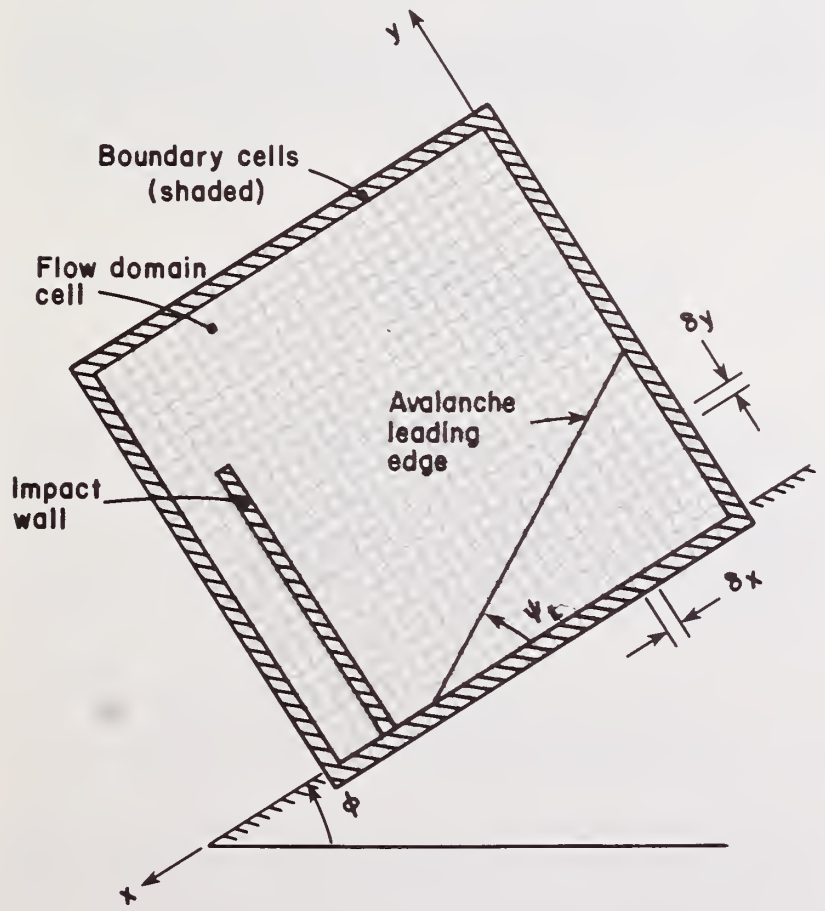

Figure 1.—Arrangement of finite difference grid, avalanche leading edge, and slope-normal impact wall.

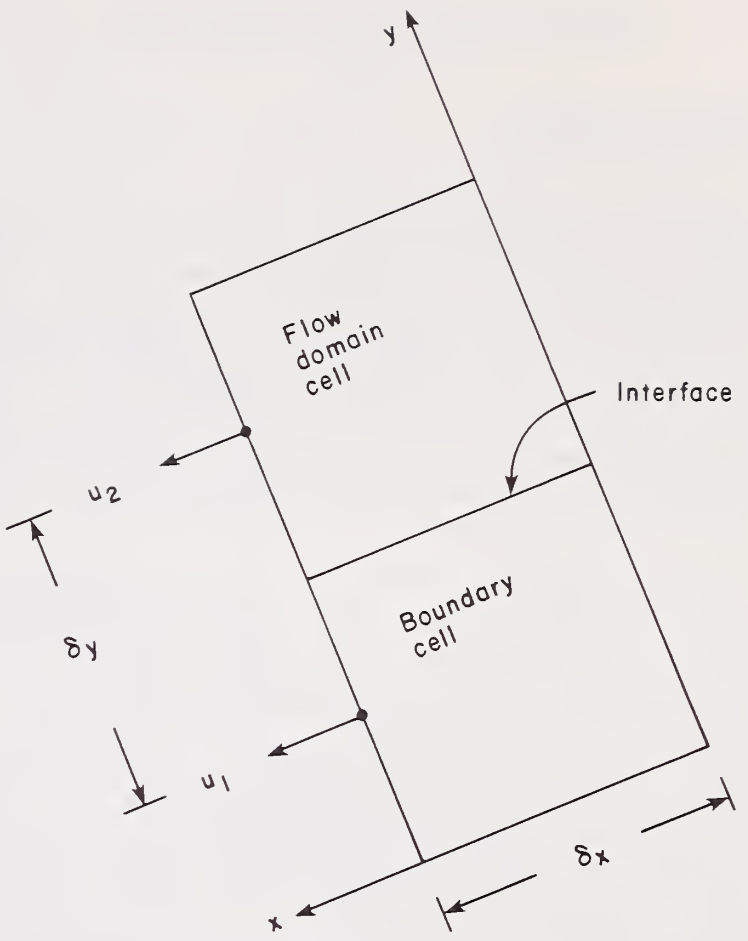

Figure 2.—Boundary cell representation.

Angle ϕ is the angle of the slope on which the avalanche advances. Angle ψ_L is the initial angle of the leading edge of the avalanche, which is assumed to be straight. Parameters δ_x and δ_y are the x and y dimensions, respectively, of an individual cell of the uniform grid. Surface friction is defined by specifying the x component of velocity in the lower boundary cell using the Newtonian shear law. If u_2 is the x component of velocity in the lowest flow domain cell, and u_1 is the corresponding velocity in the lower boundary cell (fig. 2), then

$$u_1 = u_2\ (1 - 2f) \qquad [4]$$

where f is the friction coefficient.
If $f = 0$, then $u_1 = u_2$ and the boundary is slip-free.
If $f = 1$, then $u_1 = -u_2$ and velocity at the interface between the cells is zero, which is a no-slip condition. The friction coefficient is related to shear stress at the interface, as follows:

$$\frac{\tau_{xy_0}}{\varrho} = \nu\frac{\partial u}{\partial y} \cong \nu\left(\frac{u_2 - u_1}{\delta_y}\right) = \nu\left(\frac{2u_2 f}{\delta_y}\right) \qquad [5]$$

Finally, friction coefficient, f, is assigned to each lower boundary cell individually, so that friction may vary along the slope, depending upon physical circumstances of the problem.

In the remainder of this paper, set $\nu = 0.5$ m^2/s and $f = 0.5$, as representative of nominal values for these parameters.

Impact Upon a Slope-Normal Wall

Problem Definition

Much of the experimental data from load cell measurements are taken from test structures in which the sensing elements are arrayed in a line normal to the slope surface. Thus, direct comparison of experimental data and computer simulation data is possible using a slope-normal wall (i.e., a wall perpendicular to the local slope). This geometry is also the simplest case to model using computer code AVALNCH, since the wall representation amounts to a zeroing of velocity components in a single column of cells (fig. 1).

Computer definition of the problem is shown in figure 1. The avalanche leading edge is initially defined by angle ψ_L, and material in all cells to the left of the leading edge are given an initial slope-parallel speed in the range of equilibrium speed for avalanche flow on a slope of angle ϕ. This initial assumption is not correct; but in the first cycle of computations to establish mass continuity, the velocity and pressure values in each cell are adjusted to meet specified compatibility requirements. This results in a change of shape of the leading edge profile from a straight line to other shapes, examples of which are given later as part of the presentation of data. If the initial assumption of slope-parallel speed is close to the nominal speed for a slope of angle ϕ, and with the assumed values for surface friction and viscosity, then the compatibility correction is small. What ensues is a flow in which the leading edge changes shape, but for which the nominal speed of the entire mass does not systematically change with advance of the flow. In all cases, computer runs were made with different initial velocity estimates until the flow showed the persistence in velocity as described above.

Under the driving attraction of gravity, the avalanche flows down the slope, impacts the obstacle, and piles up against it. The numerical algorithm used in program AVALNCH does not admit representation of flow over the top of the obstacle, so, consideration is limited to initial buildup of the impacting snow. A more intricate computer code that admits the overflow condition is being adapted to avalanche flow.

Force Computations

An important consideration is the definition of the resultant forces that act on the impacted wall, as computed from velocity and pressure data determined for each cell. A free body diagram of the normal and shear forces that act between a cell in the i^{th} column and j^{th} row and the wall is shown in figure 3. Also defined are the cell velocity components and the resultant base forces F_N and F_S, and base moment, M_B, needed for equilibrium at the wall. In the case of the slope-normal wall, for the i^{th} column of cells,

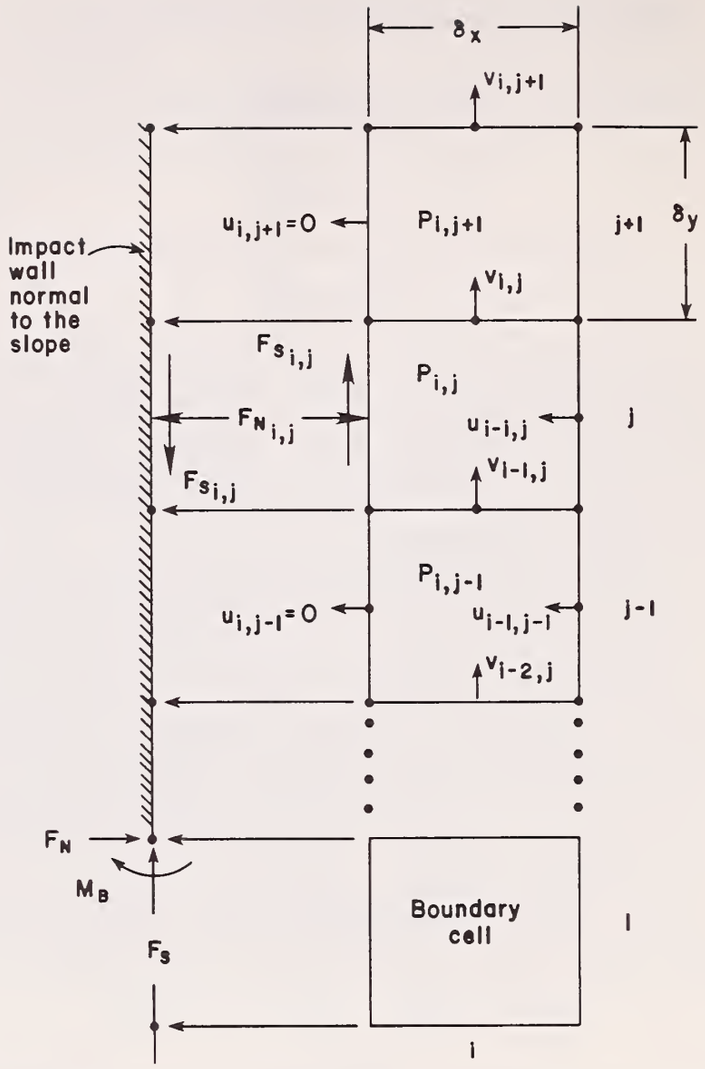

Figure 3.—Parameters and geometry of cells at the impact wall.

$$\frac{M_B}{\varrho} = \sum_{j=2}^{n} \left(\frac{F_{N_{i,j}}}{\varrho} \right) \cdot \delta_y \cdot (j - 1.5) \qquad [6]$$

The upper limit on the sum, n, is the number of cells in the i^{th} column that contains snow. For the top cell that contains snow it may be necessary to use a partial height rather than δ_y in equation 6.

For cell (i, j) the normal force on the wall, using equation 3, is:

$$\frac{F_{N_{i,j}}}{\varrho} = \left(\frac{p_{i,j}}{\varrho} \right) \delta_y - 2\nu \left(\frac{u_{i,j} - u_{i-1,j}}{\delta_x} \right) \delta_y \qquad [7]$$

where $(p_{i,j}/\varrho)$ is the actual quantity computed as "pressure" in AVALNCH. The forces reported are also scaled to unit density by equation [7] so that the units of the term in equation [7] are (m^4/s^2), which assumes force is per unit distance in the third coordinate direction. Total normal force on the wall is then

$$\frac{F_N}{\varrho} = \sum_{j=2}^{n} \frac{F_{N_{i,j}}}{\varrho} \qquad [8]$$

Various options can be exercised in computing shear stress (and also shear force). One possibility, which is based on the assumption of a no-slip wall, and a local finite difference definition of the derivatives for shear stress in equation [3] is:

$$\frac{F_{S_{i,j}}}{\varrho} = \nu\left(\frac{u_{i-1,j} - u_{i-1,j-1}}{\delta_y} + \frac{u_{i-1,j+1} - u_{i-1,j}}{\delta_y}\right)\frac{\delta_y}{2}$$

$$+ \nu\left(\frac{v_{i+1,j} + v_{i+1,j-1}}{\delta_x} - \frac{v_{i,j} + v_{i,j-1}}{\delta_x}\right)\delta_y$$

Recognizing zero terms and cancelations in this equation, it reduces to

$$\frac{F_{S_{i,j}}}{\varrho} = \frac{\nu}{2}(u_{i-1,j+1} - u_{i-1,j-1}) - \nu(v_{i,j} + v_{i,j-1}) \qquad [9]$$

Alternately, by a coarser grid averaging in which a single shear stress is defined for each cell, the following shear force for cell (i,j) is defined

$$\frac{F_{S_{i,j}}}{\varrho} = \frac{\nu}{4}(u_{i-1,j+1} - u_{i-1,j-1}) - \frac{\nu}{4}(v_{i-1,j} + v_{i-1,j-1}) \qquad [10]$$

Although a number of finite-difference methods can be used to define shear stress, equation [9] is used in subsequent evaluations. Using equation [10] implies a surface friction, f, of 0.5, whereas equation [9], with the no-slip condition, implies $f = 1.0$. Total shear force on the wall is then

$$\frac{F_S}{\varrho} = \sum_{j=2}^{n} \frac{F_{S_{i,j}}}{\varrho} \qquad [11]$$

Summary and Evaluation of Data for a Slope-Normal Wall

Setup of the problem is shown in figure 1. The total flow domain is modeled by 30 cells along the slope, and 30 cells normal to the slope. All cells are squares 0.05 m on a side. The slope-normal wall is placed in cell number 24, and the leading edge of the avalanche, at the start of flow, is in cell number 21.

Output from program AVALNCH consists of a listing of the pressure per unit density, velocity components, and flow height for each cell at any specified time during the impact. Forces, F_N/ϱ and F_S/ϱ, moment, M_B/ϱ, and maximum pressure, p_M/ϱ, are computed at each time increment of the computations and are listed sequentially. A typical impact condition is considered to outline the results. Slope angle was set at $\phi = 30°$, leading edge angle $\psi_L = 30°$, nominal slope-parallel

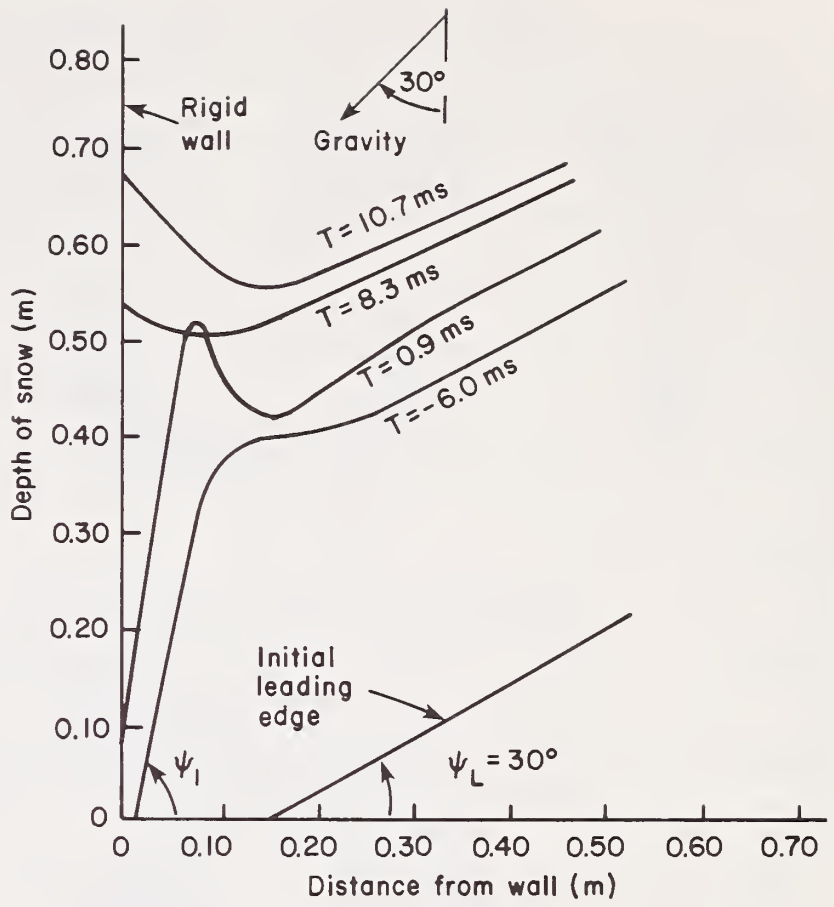

Figure 4.—Distribution of snow upslope from a rigid slope-normal wall of several times measured from time of impact at T = 0.0 s. Slope angle = 30°. Impact velocity = 20 m/s. Kinematic viscosity = 0.5 m²/s. Friction coefficient = 0.5.

flow velocity $U_o = 20$ m/s, and viscosity and friction at $\nu = f = 0.5$. One type of result is the change of shape of the leading edge of the avalanche as the flow progresses (fig. 4). At the instant of impact, the leading elements of the flow have changed from an initial angle of $\psi_L = 30°$, to an impact angle $\psi_I = 76°$. After initial contact, the avalanche front piles against the slope-normal wall with a profile sequence as depicted in figure 4. Maximum pressure and maximum normal force on the wall occur when the flow surface is approximately parallel to the slope (at T = 8.3 ms, for this case). The time histories of the normal and shear forces and the moment at the base of the wall are shown in figure 5. It is seen that a sharp peak in normal force occurs at approximately 8.3 ms into the impact, and persists for approximately 1.5 ms.

The distribution of pressure along the slope-normal wall for the various times into the impact, corresponding to the different snow profiles of figure 4, are shown in figure 6. The pressure distribution corresponding to T = 8.3 ms is 0.1 ms off the time at which the pressure is maximum for the entire impact, at $p_M/\varrho = 2{,}500$ m²/s². Maximum pressure was found to vary with the angle of the leading edge of the avalanche, ψ_L. As ψ_L is changed, the impact angle ψ_I also changes according to the results listed in table 1. Although leading edge angle is more than doubled, impact angle changes by only 13°, but with the angle approaching 90°. Thus, the slope of the frontal face of the avalanche at impact has a pronounced affect on maximum pressure and total force exerted on the wall.

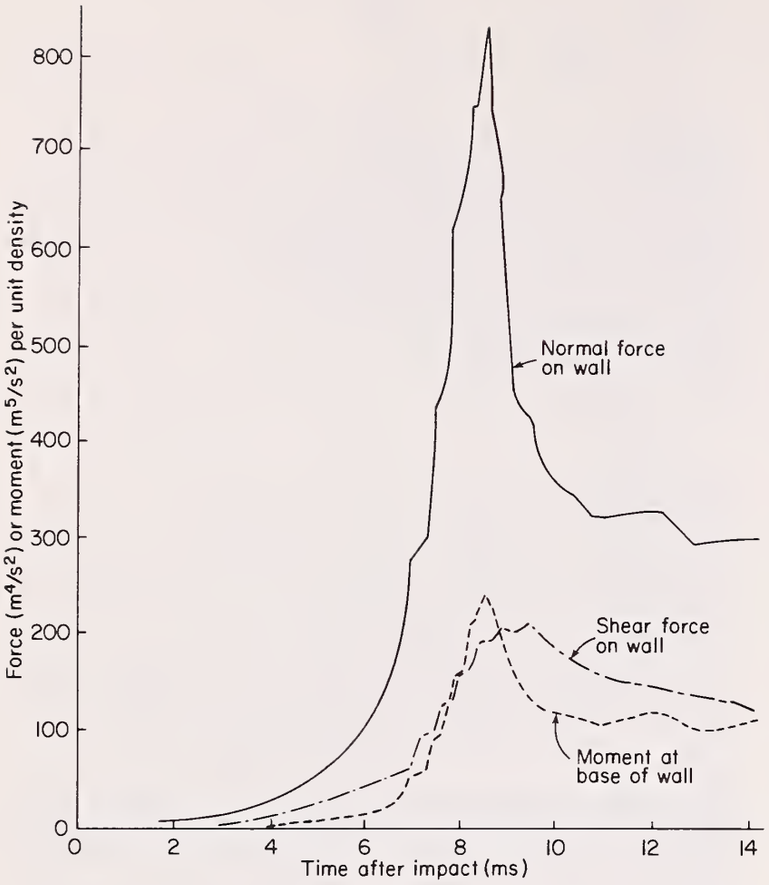

Figure 5.—Force and moment components as functions of time after impact upon a slope-normal wall. Slope angle = 30°. Initial leading edge angle = 30°. Impact velocity = 20 m/s. Kinematic viscosity = 0.5 m²/s. Friction coefficient = 0.5.

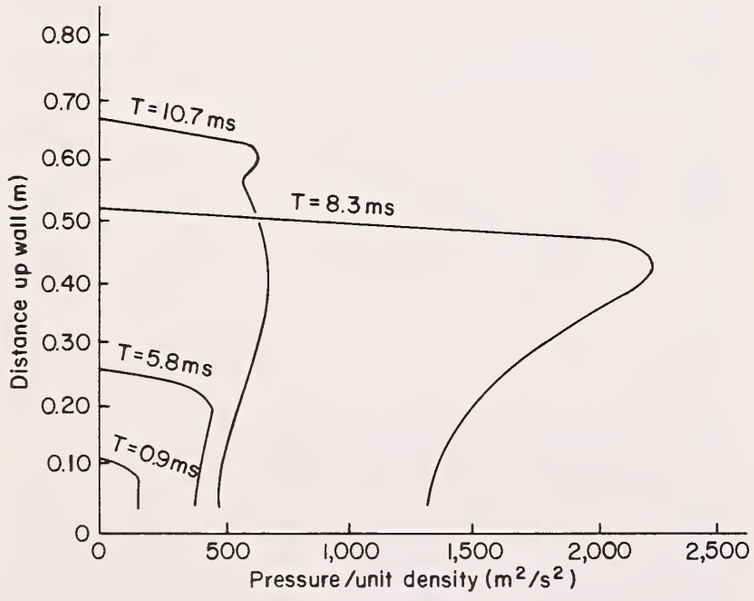

Figure 6.—Distribution of pressure per unit density along slope-normal wall at several times measured from time of impact at T = 0.0 s.

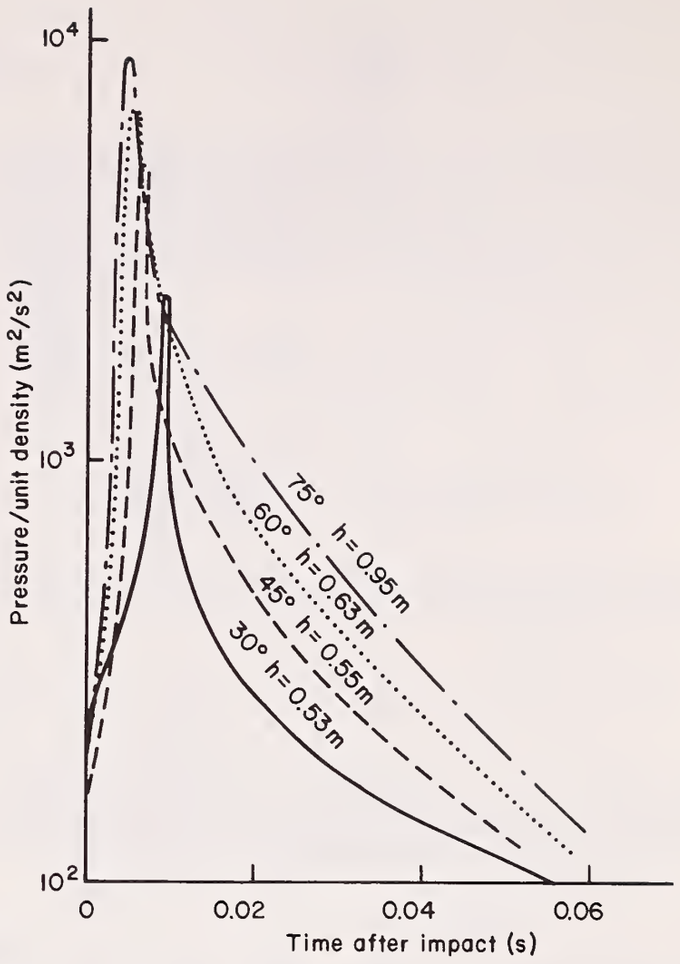

Figure 7.—Pressure profile at height of maximum pressure on wall versus time after impact for avalanche leading edge angles of 30°, 45°, 60°, and 75°.

Using the largest value of maximum pressure per unit density of 9,700 m²/s² (table 1), convert this to an actual pressure value by assuming a nominal snow density of 300 kg/m³ so that

$$P_{act} = \varrho p_M = \left(9{,}700\ \frac{m^2}{s^2}\right)\left(300\ \frac{kg}{m^3}\right)$$

$$= 2{,}910{,}000\ kg/ms^2 \text{ or } N/m^2$$
$$= (2{,}910{,}000\ N/m^2)\ (1\ kg/9.807N)\ (1\ ton/1{,}000\ kg)$$
$$p_{act} = 297\ ton/m^2$$

which is approximately a factor of 10 greater than experimentally measured pressures which are in the range of 30 t/m² as noted in the introduction.

From the physical measurements reported by Schearer (1973), maximum pressure is associated with time durations on the order of 0.1 second. This occurs because of the relatively long time constant of the load-cell type sensor used to monitor force. Thus a pressure peak of 1.5 ms duration would not be detected except in an averaging sense. Therefore, it is necessary to consider the pressure distribution over 0.1 second duration in the analytical results in order to make comparison with experimental data. To this end, the pressure distribution at the height of maximum pres-

Table 1.—Variation in maximum pressure and forces as a function of leading edge angle, ψ_L, for the slope-normal wall geometry

Leading edge angle, ψ_L	Estimated impact angle, ψ_I	Maximum pressure per unit density	Maximum normal force per unit density	Maximum shear force per unit density	Maximum bending moment per unit density
degrees	*degrees*	m^2/s^2	m^4/s^2	m^4/s^2	m^5/s^2
30	76	2,500	830	200	240
45	81	4,700	1,750	320	500
60	81	6,700	2,800	500	1,000
75	86	8,700	5,800	1,300	3,600
80	88	9,700	7,200	1,600	5,000

Table 2.—Average pressure on the wall at the height of maximum pressure for different leading edge angles and for a nominal flow velocity of 20 m/s

Leading edge angle	Average pressure per unit density[1]	Average pressure[2]	Height on wall of maximum pressure	Maximum pressure[2]
degrees	m^2/s^2	ton/m^2	*m*	ton/m^2
30	305	9.3	0.53	76.5
45	455	13.9	0.55	144
60	600	18.4	0.63	205
75	815	25.0	0.95	266
80	850	26.0	1.25	297

[1]*Based on 0.1-s time duration since impact.*
[2]*Based upon snow density of 300 kg/m³.*

sure on the wall for four different cases is shown in figure 7. From these data the average pressure can be determined from the area under each curve. The computed values, and the conversion to actual pressures, assuming a snow density of 300 kg/m³, are listed in table 2.

By averaging pressure over 0.1 s, it is seen that computed pressures fall in the same range as experimentally measured pressures. Plotting maximum and average pressures as functions of the estimated impact angles (fig. 8), linear variation, particularly of average pressure, is a good approximation. It should be noted that computation of impact angle is approximate in that the 0.05- by 0.05-m grid assumed in determining these results is not adequate for detailed resolution of the leading edge shape. Because of this limitation, impact angle is based upon straight line approximations of leading edge shape, as depicted in figures 4, A-1, A-3, and A-5.

By changing the angle of the ground surface, avalanches with different nominal flow velocities can be modeled. By doing this, flow velocities of $U_0 = 7$, 10, 15, and 30 m/s were modeled at initial leading edge angles of 30°, 45°, 60°, and 75°. For any given initial leading edge angle, the impact angle for all flow speeds was found to be approximately the same as that reported for the 20 m/s case (table 1). Thus, using different values

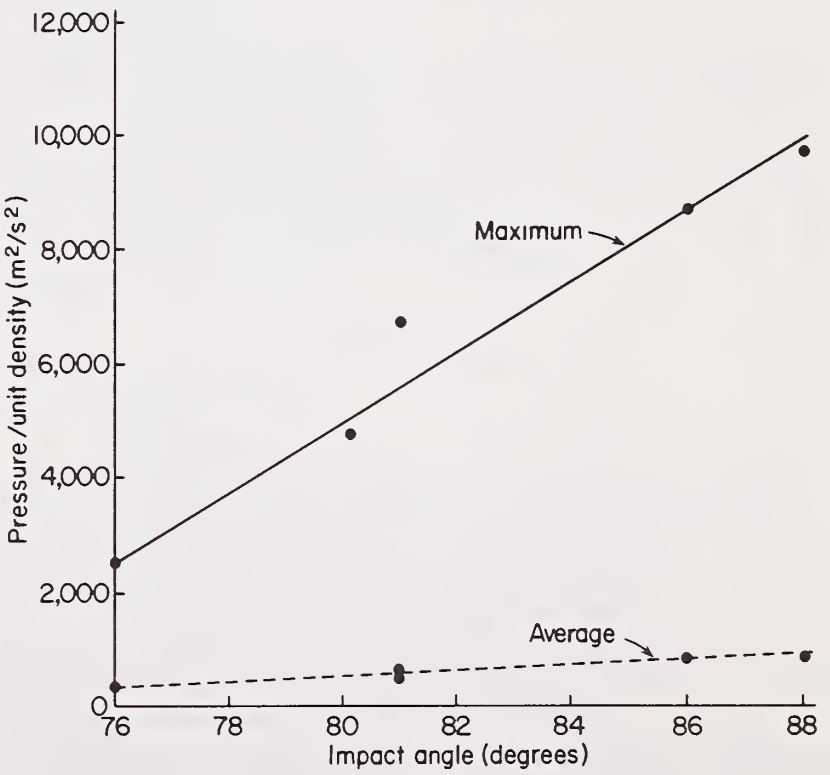

Figure 8.—Variation in maximum and average pressures with estimated leading edge angle for imapct at 20 m/s onto a slope-normal wall. Kinematic viscosity = 0.5 m²/s. Friction coefficient = 0.5.

of leading edge angle at impact, the variation in maximum and average pressure versus the nominal flow speed of the avalanche is shown in figure 9. Results obtained for $U_0 = 7$ m/s show no pressure peak, but rather a monotonic increase in pressure as the snow piles against the wall.

A surface undulation of the snow profile after impact subsides approximately 0.2 m upslope from the impacted wall (fig. 4). Farther upslope from this station, the particles at the surface advance at the nominal speed of 20 m/s. It can be hypothesized that the height of snow at the terminal point of the undulation is representative of the height needed to produce the maximum (or average) pressure of the impact, dependent also upon impact angle. These observed flow heights are summarized for the different nominal flow speeds and impact angles in figure 10. Combining the results of figures 9 and 10 led to the conclusion, for example, that an avalanche moving at 20 m/s and having a nominal leading edge angle at impact of $\psi_I = 76°$, will produce an average pressure of 300 m²/s² per unit of density, a maximum pressure of approximately 2,500 m²/s² per unit of density, and an equivalent flow height of 0.55 m.

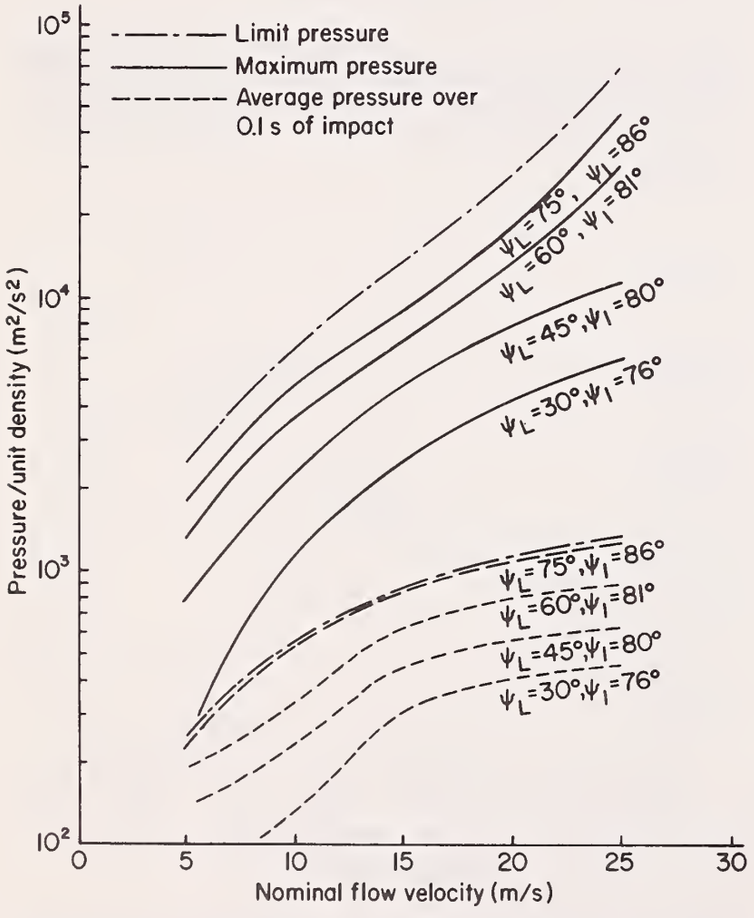

Figure 9.—Variation in pressure versus nominal flow velocity for different leading edge angles at impact with a slope-normal wall.

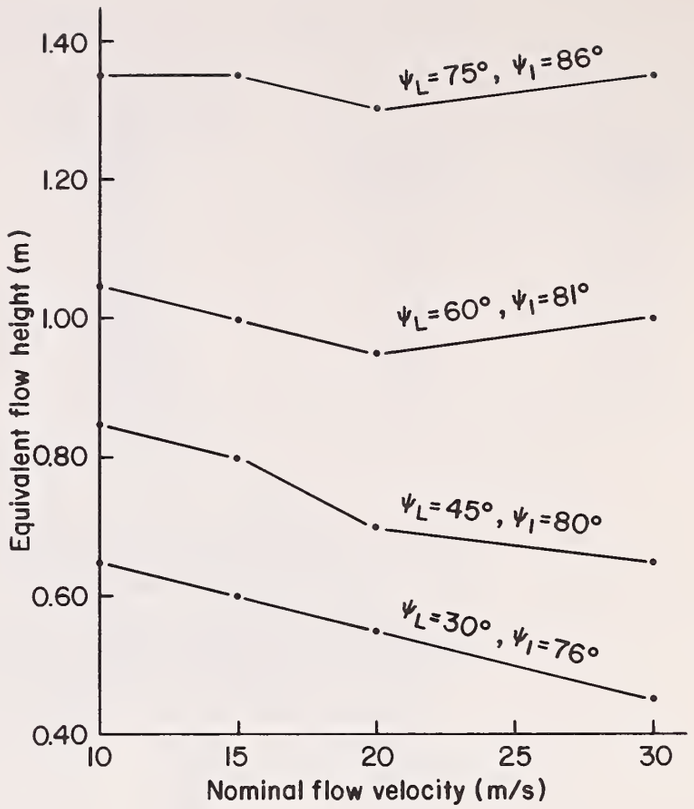

Figure 10.—Equivalent flow height versus nominal flow velocity for different leading edge angles at impact with a slope-normal wall.

Impact Upon a Vertical Wall

Problem Description

The vertical wall case represents the geometry when an avalanche impacts against a building or similar type structure. Again, only a two-dimensional approximation of the flow, on what would likely be a three-dimensional problem unless the structure and avalanche are broad, is considered.

As in the slope-normal case, the avalanche is depicted by a constant slope leading edge starting in cell number 21 of a 30 by 30 grid. The case of a nominal flow velocity of 20 m/s is considered to compare maximum pressure and average pressure with the slope-normal case. If differences are not large, then the cost of duplicate computer studies of the vertical wall case are not necessary, and reference can be made to the results of the section on governing equations and flow parameters as typical for both cases. A nominal flow velocity of 20 m/s corresponds to equilibrium flow on a slope of 30°. Thus, to specify a vertical wall, zero velocity cells must be specified in an array as shown in figure 11. Starting at the bottom surface of the grid the 2-2-1 sequencing of steps toward the uphill averages to an equivalent vertical wall.

Listing of the computer code for the vertical wall case is given in Appendix B. Substitute instructions are also inserted for the case of the slope-normal wall. For problem arrays other than 30 by 30 the DIMENSION

statement of lines 9 and 10 must be changed. For a nominal impact speed other than 20 m/s, instruction 112 must be changed. If the leading edge of the avalanche is not to start in cell 21, then instruction 110 changes. All remaining data for this code, particularly the input data, is the same as described for program AVALNCH (Lang et al. 1979). Specifically, input instructions are 13, 19, 65, 66, and 68, for which description of the parameters and arrays are given in Appendix A (Lang et al. 1979).

Force Calculations

For the vertical wall geometry it is necessary to distinguish between an open cell and a corner cell (fig. 11). For the open cell, the calculation of normal and shear force at the interface with the wall is that specified by equations 7 and 9. For a corner cell, two normal and two shear forces are specified on the two adjacent fixed boundaries (fig. 12). If the cell number is *i,j* corresponding to the column and row number, respectively, then the normal forces are computed from the equations

$$\frac{F_{N_1}}{\varrho} = \left(\frac{P_{i,j}}{\varrho} \right) \delta_y - 2\nu \left(\frac{u_{i,j} - u_{i-1,j}}{\delta_x} \right) \delta_y \qquad [12]$$

$$\frac{F_{N_2}}{\varrho} = \left(\frac{P_{i,j}}{\varrho} \right) \delta_y - 2\nu \left(\frac{v_{i,j} - v_{i,j-1}}{\delta_y} \right) \delta_x \qquad [13]$$

where the subscripts follow the order as depicted in figure 3. The two shear forces for the cell are computed by the equations:

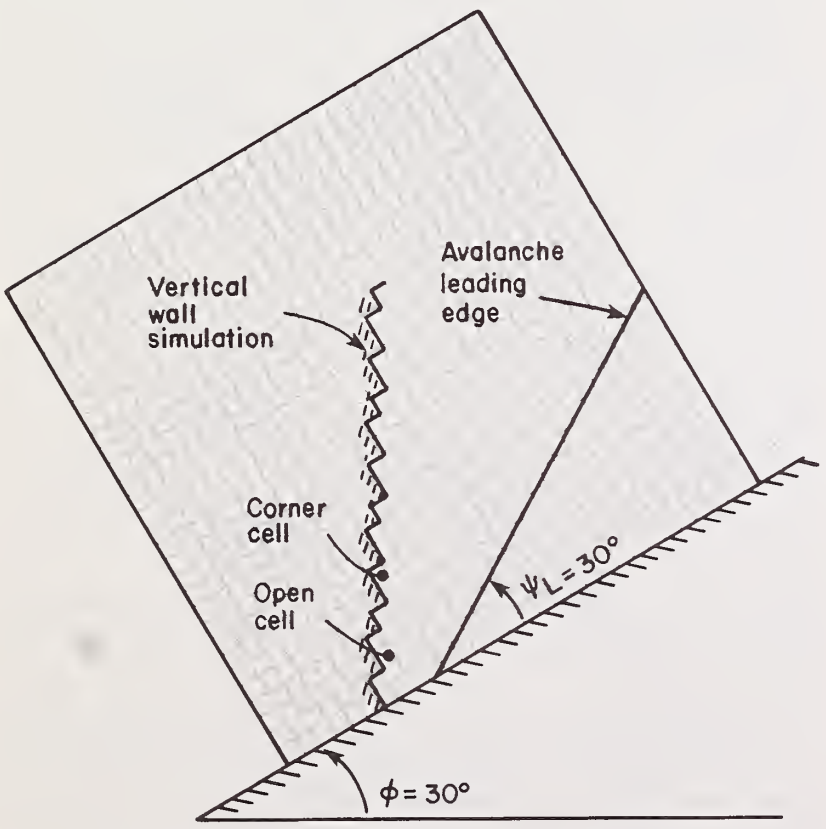

Figure 11.—Grid array and wall geometry for vertical wall impact. Case shown is a 30° slope, for which nominal flow speed is 20 m/s and leading edge angle is $\psi_L = 30°$.

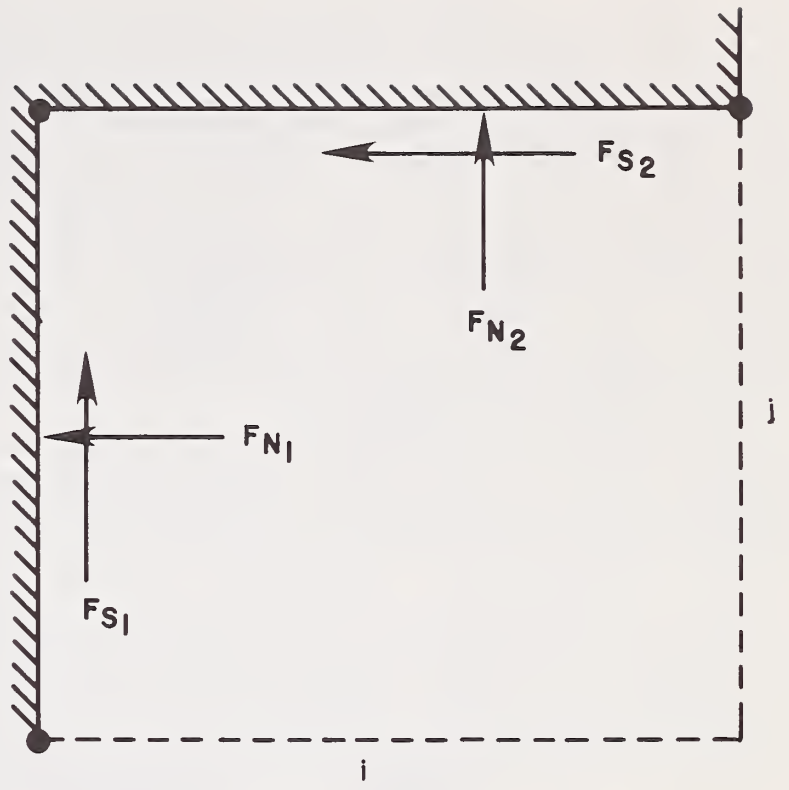

Figure 12.—Forces acting on the boundary of corner cell i, j.

$$\frac{F_{S_1}}{\varrho} = -\frac{\nu}{2}(u_{i-1,j-1} + v_{i,j-1})$$

$$\frac{F_{S_2}}{\varrho} = -\frac{\nu}{2}(u_{i-1,j} + v_{i-1,j-1}) \qquad [14]$$

where $\delta_x = \delta_y$ has resulted in simplification of these equations.

By summing the respective slope-parallel and slope-normal forces of each cell over all cells that contain snow, the total slope-parallel and slope-normal forces are obtained. Total moment at the base of the wall must necessarily include the moment of all force components F_{N_1}, F_{S_1}, F_{N_2}, and F_{S_2} of a corner cell, and F_N and F_S of an open cell as the cells are offset in moving vertically upward.

Summary and Evaluation of Data for a Vertical Wall

The pressure variations at the height of maximum pressure for the four cases of leading edge angles of $\psi_L = 30°$, 45°, 60°, and 75° are shown in figure 13. The evaluation is for the case of a nominal impact velocity $U_o = 20$ m/s, kinematic viscosity $\nu = 0.5$ m²/s, friction at $f = 0.5$, and a slope angle $\phi = 30°$. These values are selected so that the flow in the mainstream of the advancing avalanche is equilibrium flow.

For the case of the vertical wall geometry, the angle between the wall and the upslope ground surface is 60°. For the avalanche cases considered, leading edge angles increase rapidly, and all angles at the instant of impact for the slope-normal geometry equal or exceed $\psi_I = 76°$. At these angles of the leading edge in the case of a vertical wall, upper reaches of the leading edge

will contact the wall before the base. This is in contrast to the occurrence in the slope-normal wall geometry in which initial contact is at the base. Thus, different pressure and force histories can be expected for the two geometries. Maximum pressures and average pressures over the initial 100-ms duration of impact as functions of leading edge angle are given in table 3 for the vertical wall geometry. Although peak pressures show a wide variation among the different cases, average pressure varies by less than a factor of 2.0. This is verified by the near equality of areas under the pressure-time curves of figure 13.

Detailed variations in normal force, shear force, and bending moment on the wall for the case of the 30°, leading edge angle avalanche are shown in figure 14. Similar plots for the cases of leading edge angles of 45°, 60°, and 75° are presented in Appendix A (figs. A-7, A-8 and A-9). No attempt is made at plotting the snow surface distribution for the vertical wall case because of uncertainty as to the area of contact at the leading edge as a function of time. To accurately evaluate contact area as a function of time requires only refinement in the finite-difference grid, which is technologically straightforward. Results, at least for the case of $\psi_L = 30°$, show that maximum pressure and force on the vertical wall occur when the impacting snow front piles up until the snow surface is approximately parallel to the ground surface next to the impact surface. This is consistent with the results obtained also for the slope-normal wall.

Table 3.—Variation in pressures as functions of leading edge angle for the vertical wall geometry

Leading edge angle	Maximum pressure per unit density	Average pressure per unit density[1]	Average pressure[2]
degrees	*m^2/s^2*	*m^2/s^2*	*ton/m^2*
30	730	280	8.6
45	1,200	320	9.8
60	2,200	340	10.4
75	10,600	450	13.8

[1]Average pressure over initial 100 ms of impact.
[2]Based upon snow density weight of 3,000 kg/m^3.

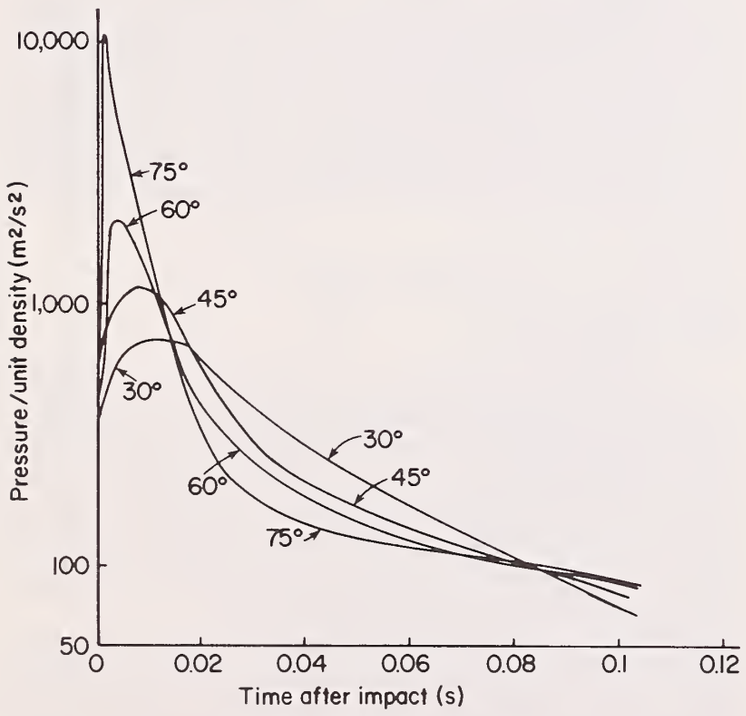

Figure 13.—Pressure profile on vertical wall versus time after impact for avalanche leading edge angles of 30°, 45°, 60°, and 75°. Nominal flow velocity is U_0 = 20 m/s. Kinematic viscosity = 0.5 m^2/s. Friction coefficient = 0.5.

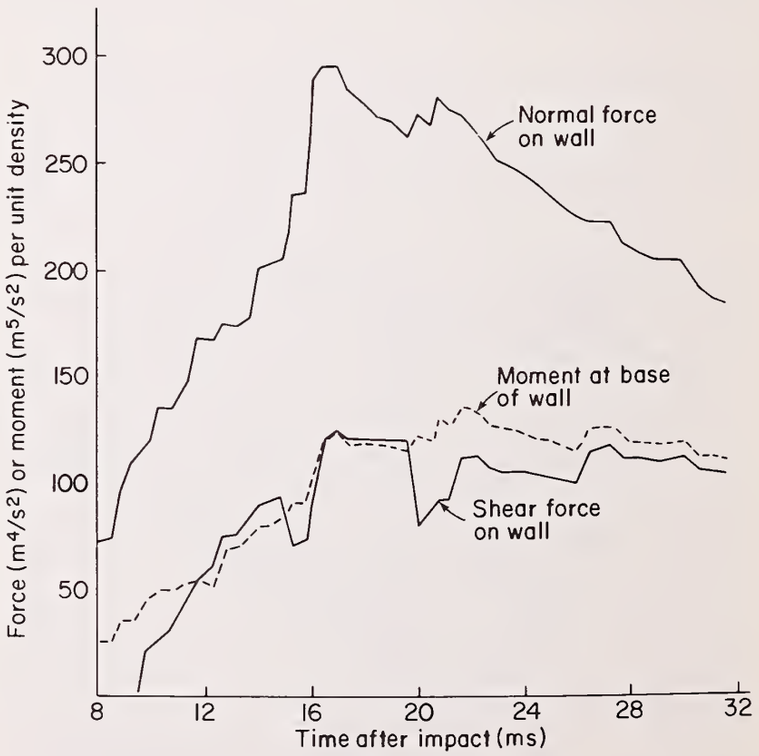

Figure 14.—Force and moment components as functions of time after impact on a vertical wall. Slope angle = 30°. Initial leading edge angle = 30°. Impact speed = 20 m/s. Kinematic viscosity = 0.5 m^2/s. Friction coefficient = 0.5.

Table 4.—Average and maximum pressures generated on slope-normal and vertical walls as a function of leading edge impact angle, ψ_l, and for a nominal flow velocity of 20 m/s at impact

Leading edge impact angle	Slope normal wall		Vertical wall	
	Maximum pressure per unit density	Average pressure[1] per unit density	Maximum pressure per unit density	Average pressure[1] per unit density
degrees	m^2/s^2	m^2/s^2	m^2/s^2	m^2/s^2
76	2,500	305	730	280
80	4,700	455	1,200	320
81	6,700	600	2,200	340
86	8,700	815	10,600	450
88	9,700	850	—	—

[1]*Averaged over initial 100 ms of impact.*

Conclusions from Slope-Normal and Vertical Wall Results

Although the computer solutions include calculations of forces and moments on the slope-normal and vertical walls (which is essential information for design), pressure is the fundamental quantity for comparison of the two cases. The average and maximum pressures per unit density for the two cases are given in table 4.

For impact angles of 76°, 80°, and 81°, the slope-normal wall pressures are larger than corresponding vertical wall pressures with larger differences noted for maximum pressures than for average pressures. For an impact angle of 86°, the vertical wall maximum pressure suddenly jumps to a value larger than the corresponding value for the slope-normal case. A plausible explanation for this is that the leading edge of the initial impacting snow is near-parallel to the wall surface at contact. The result of this is a generated maximum pressure of 10,600 m^2/s^2 per unit density that peaks and subsides in less than a millisecond (fig. A-9). This is followed by a pressure tailoff such that average pressure greater than 100 ms is comparable to that of the other impact angle cases. This wave "slapping" action, well recognized in water wave phenomenon, apparently can occur in avalanche impact also, and constitutes the extreme case in pressure generation.

To further verify this occurrence, a fifth case of impact on the slope-normal wall was run. An initial leading edge angle of 80° changes into an estimated impact angle of 88° which results in a maximum pressure of 9,700 m^2/s^2. Assuming a straight-line extrapolation on maximum (and average) pressure versus impact angle (fig. 8), the estimated limit pressure curves of figure 9 are determined for the case of a slope-normal wall. Although not explicitly verified for different nominal flow speeds, computed results indicate that limit pressures for the vertical wall case are of the same order as for the slope-normal case. Since all pressures reported include static pressure plus a velocity gradient term (equation [3]), it is expected that pressures on walls that make small angles with the ground surface would be considerably smaller than the limit pressures reported in figure 9.

It is noted also that the limit pressures cited are based upon avalanche impact with a rigid wall. Any wall flexibility can be expected to decrease the maximum pressure. Additionally, compressibility of the snow itself will also tend to decrease pressure. Neither wall flexibility nor snow compressibility are modeled in the computer representation. Note, if wave reflection inside a specific impacted structural system is considered, internal stresses may develop that are larger than the incident impact pressure.

A more systematic development of pressure peaking is noted in the slope-normal case. There is a sharp peak for all impact angles evaluated. The nominal duration of each peak is from 1.0 to 2.0 ms. Assuming the existence of this type of loading, the question arises whether a pressure pulse of this duration can have significant effect on structural materials. Results of tests on small steel specimens (Newmark and Haltiwanger 1962) show that stresses on the order of twice the yield stress, then applied rapidly, can cause material yielding and fracture within 1.0 ms. However, extrapolation of this to reinforcing steel is not apparent. Although stresses on structures may develop to values beyond yield or fracture values, strains necessary for the failure will not develop because of large inertia effects. Thus, for typical structures made of steel, concrete, or wood, it is unlikely that the millisecond duration pulse will have a significant effect, and design should be predicated upon average pressure response.

From these results we conclude that the specific shape of the leading edge of the avalanche at impact has a significant effect on the maximum pressure that is generated. A worst case geometry has been evaluated from this computer study; however, the statistical probability of its occurrence is not known. To obtain supportive data from field observations, advanced avalanche observation techniques would have to be developed that would allow penetration of the usual snow-air cloud that accompanies all but the slow-moving wet-snow avalanches.

A second recourse, although less accurate than physical measurements, would center on determining the viscous and friction parameters of the flow more accurately than what is currently the case. Then, using this information, steady state flow would be simulated on the computer, and a statistical estimate of the distribution of leading edge angle would be determined by numerical means.

A third (experimental) alternative is to use a number of sensitive pressure transducers with millisecond response capability on a rigid post and measure the relative times of pressure buildup between transducers. This provides a means for estimating the leading edge shape of the more dense flowing snow of an avalanche. From a number of such measurements, a statistical description of leading edge shape would be obtained.

Until such time that more data is available on avalanche flow, recourse to worst case design is the safest approach, although probably not very economical.

Finally, the maximum pressure peaks reported by Salm (1964) and the data given here are compared. The peaks measured by Salm were two to five times greater than average pressures reported, and the pulses show durations on the order of 5 to 10 ms. Results reported here show maximum pressure to be as much as nine times greater than average pressure and the pulses of duration 1 to 2 ms. Whereas, the computed results are for impact upon a rigid wall, the impact in Salm's experiments is against an elastic wall. Based upon physical reasoning, one would expect a decrease in pulse height and spreading of the pulse when impact is changed from a rigid to an elastic wall. Qualitative verification of this is possible in program AVALNCH by inserting a cell at the wall over which velocity is greatly reduced rather than set to zero. Although this has not been done, differences in initial peak-load characteristics between the computer results and those of Salm seem to have a plausible physical basis.

The general conclusion from these computer results is that program AVALNCH has modeling capability for avalanche impact. Uncertainties as to leading edge geometry prevent explicit ranging of expected pressures; however, preliminary results show that upper limits on pressure can be established. Further correlation between computer predictions and field observations are warranted; the types of parameters that need to be measured to provide closer correlations have been identified.

Literature Cited

Furukawa, Iwao. 1957. Impact of avalanches. Snow and Ice 29(5):140-141.

Hirt, C. W., B. D. Nichols, and N. C. Romero. 1975. SOLA: A numerical solution algorithm for transient fluid flows. 50 p. Los Alamos Science Laboratory, Los Alamos, N. Mex.

Lang, T. E., K. L. Dawson, and M. Martinelli, Jr. 1979. Numerical simulation of snow avalanche flow. USDA Forest Service Research Paper RM-205, 51 p. Rocky Mountain Forest and Range Experiment Station, Fort Collins, Colo.

Mears, A. 1975. Dynamics of dense-snow avalanches interpreted from broken trees. Geology 3(9):521-523.

Newmark, N. M., and J. D. Haltiwanger. 1962. Air Force design manual: Principles and practices for design of hardened structures. AFSWC-TDR-62-138, 638 p. National Technical Information Service No. AD-295 408, Springfield, Va.

Saito, Sotokichi, Motohiro Yoshimura, Kazuma Uto, Osamu Fukuchi, Hiroshi Nakajima, Masaaki Fujita, and Masanori Kawahara. 1963. Study on avalanche preventive steel structures. NKK Steel Note 3:57-63.

Salm, B. 1964. Anlage zur untersuchung dynamischer wirkungen von bervegtem schnee. ZAMP 15: 357-375.

Schaerer, P. A. 1973. Observations of avalanche impact pressures. p. 51-54. *In* Advances in North American avalanche technology: 1972 symposium. R. I. Perla, compiler. [Reno, Nev., November 16-17, 1972] USDA Forest Service General Technical Report RM-3, 54 p. Rocky Mountain Forest and Range Experiment Station, Fort Collins, Colo.

Shimizu, H., T. Huzioka, E. Akitaya, H. Narita, M. Nakagawa, and K. Kawada. 1973. Study on high speed avalanche in Kurobe Canyon III. Low Temperature Science A(32):126 [English summary].

Voellmy, A. 1964. On the destructive force of avalanches. Translation 2, 64 p. USDA Forest Service, Alta Avalanche Studies Center, Utah. [Available from Rocky Mountain Forest and Range Experiment Station, Fort Collins, Colo.]

Appendix A

Supplemental Plotted Data

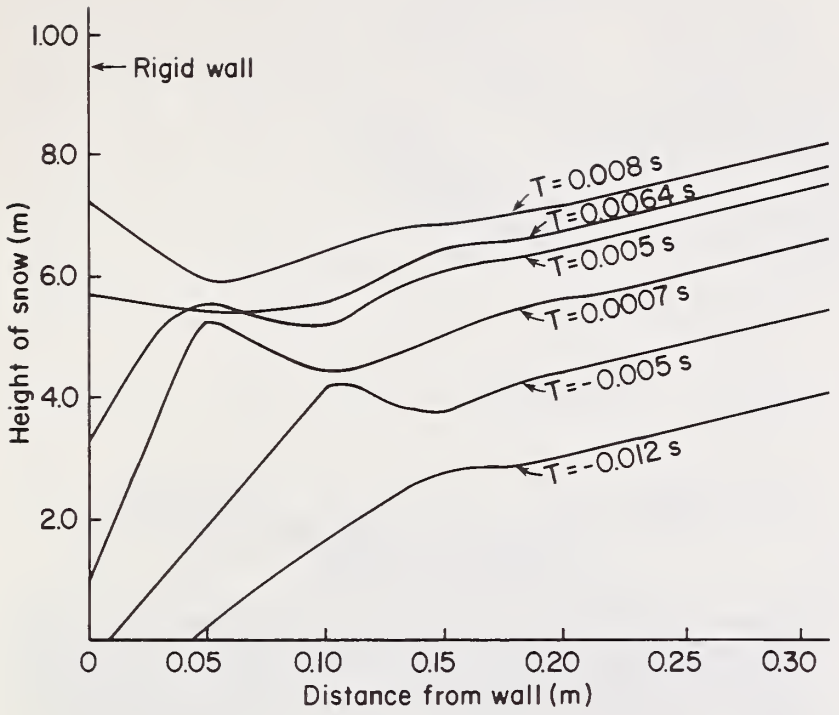

Figure A-1.—Distribution of snow upslope from rigid impact wall at several times measured from time-of-impact at T = 0.0. Slope angle = 30°. Leading edge angle = 45°. Flow velocity = 20 m/s. Kinematic viscosity = 0.5 m²/s. Friction coefficient = 0.5.

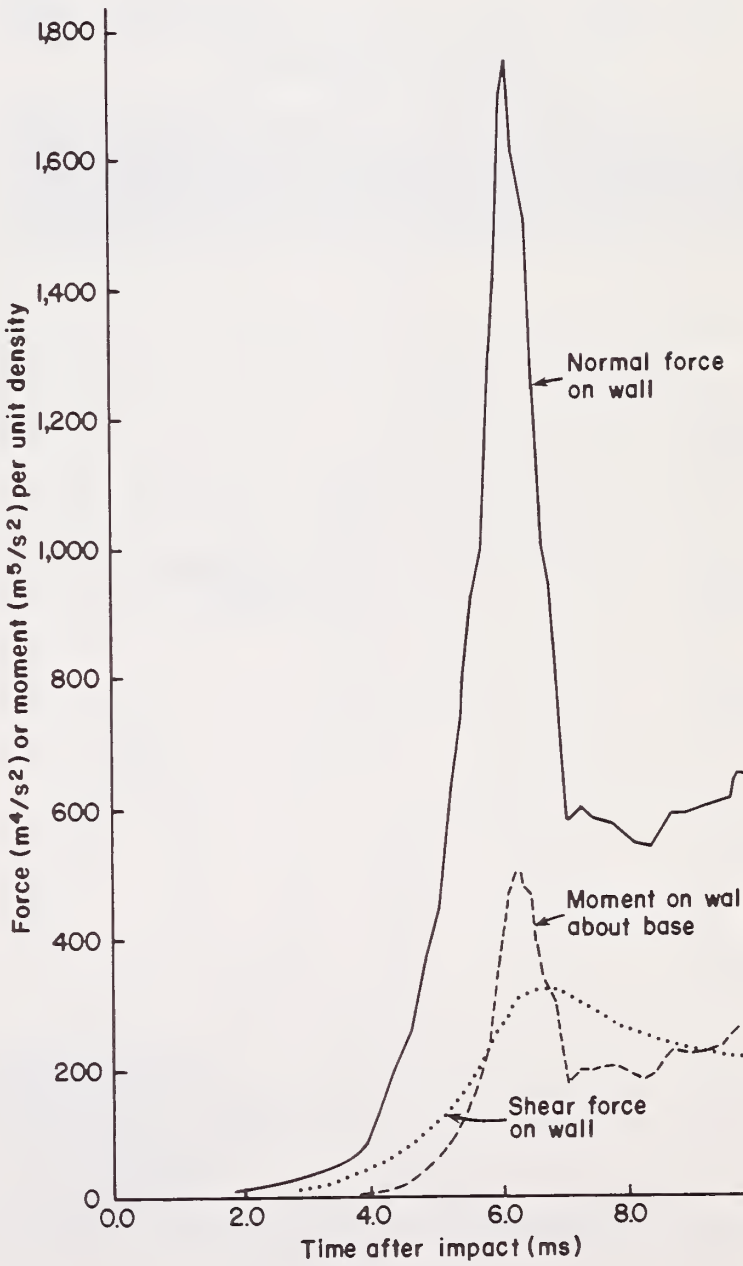

Figure A-2.—Force and moment components as functions of time after impact on a slope-normal wall. Leading edge angle=45°. Flow velocity=20 m/s. Kinematic viscosity=0.5 m²/s. Friction coefficient=0.5.

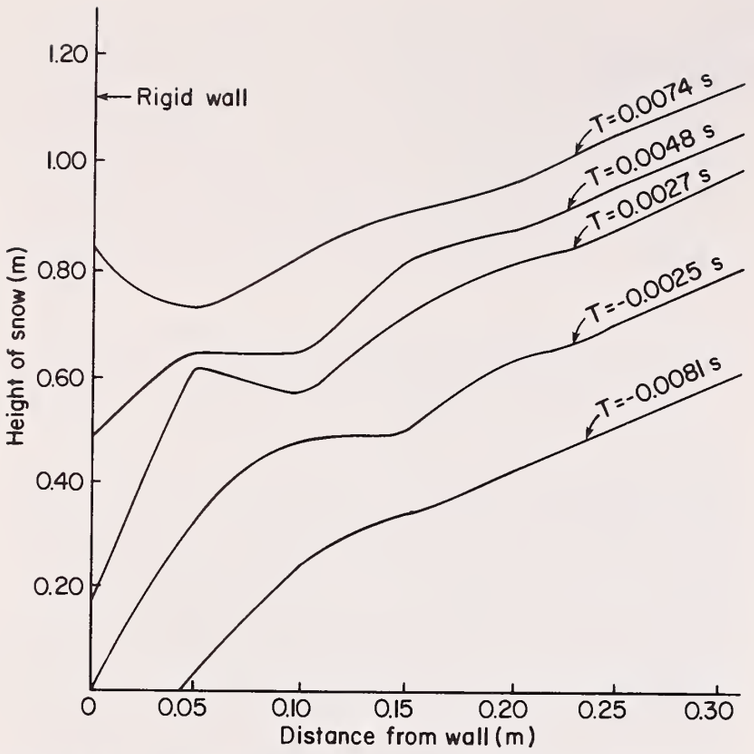

Figure A-3.—Distribution of snow upslope from rigid impact wall at several times measured from time-of-impact at T = 0.0. Slope angle = 30°. Leading edge angle = 60°. Flow velocity = 20 m/s. Kinematic viscosity = 0.5 m²/s. Friction coefficient = 0.5.

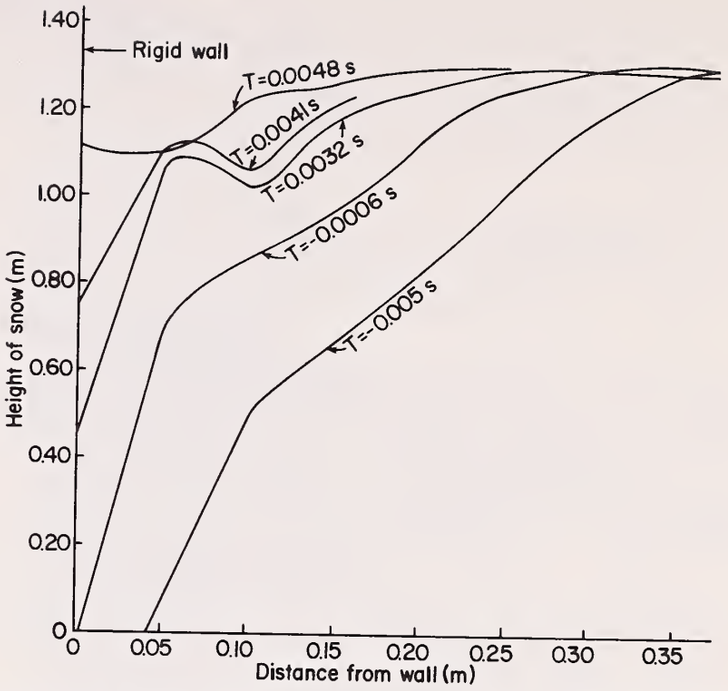

Figure A-5.—Distribution of snow upslope from rigid impact wall at several times measured from time-of-impact at T = 0.0. Slope angle = 30°. Leading edge angle = 75°. Flow velocity = 20 m/s. Kinematic viscosity = 0.5 m²/s. Friction coefficient = 0.5.

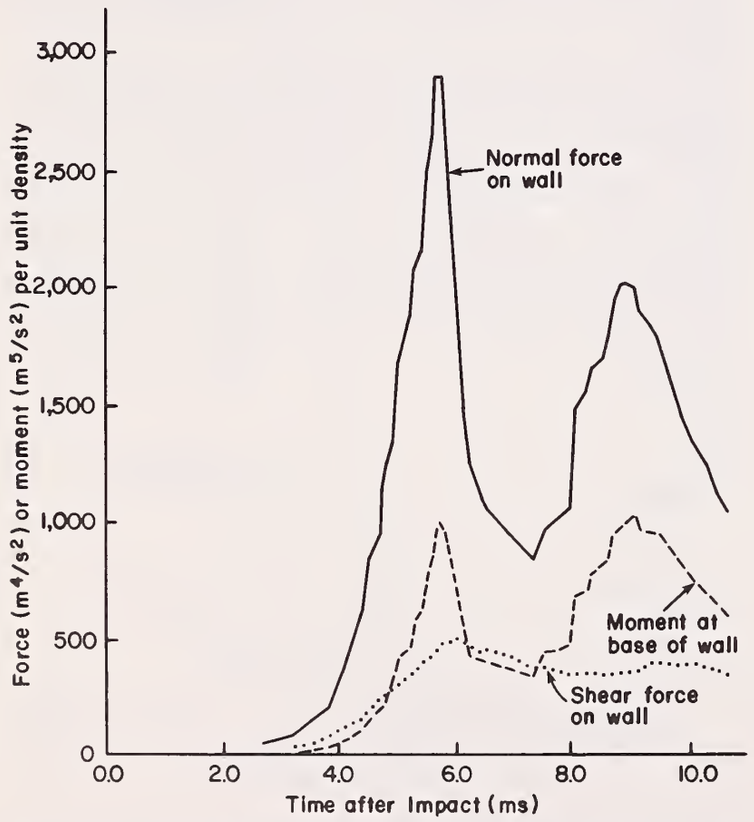

Figure A-4.—Force and moment components as functions of time after impact on a slope-normal wall. Leading edge angle = 60°. Flow velocity = 20 m/s. Kinematic viscosity = 0.5 m²/s. Friction coefficient = 0.5.

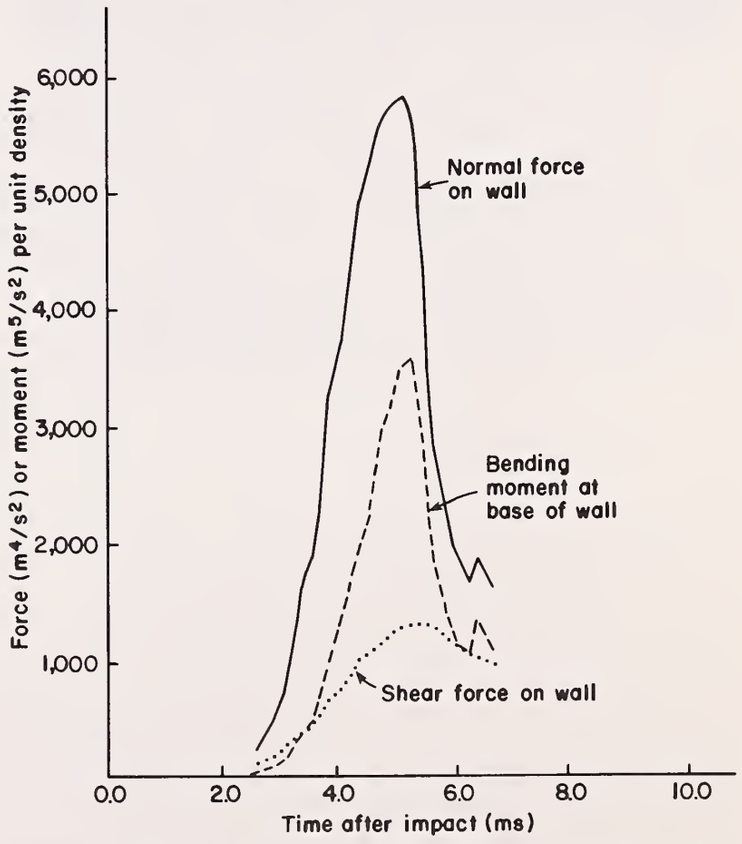

Figure A-6.—Force and moment components as functions of time after impact on a slope-normal wall. Leading edge angle = 75°. Flow velocity = 20 m/s. Kinematic viscosity = 0.5 m²/s. Friction coefficient = 0.5.

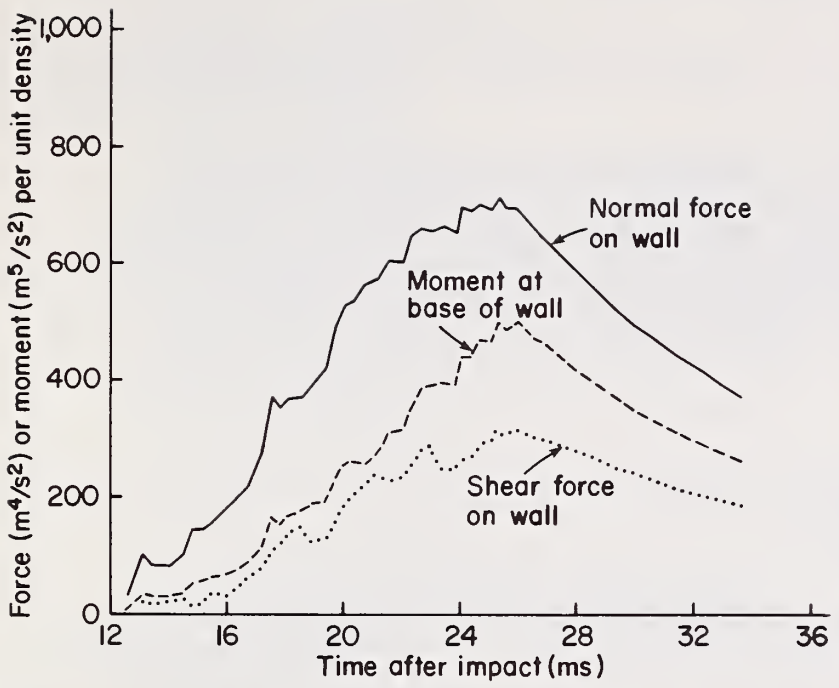

Figure A-7.—Force and moment components as functions of time after impact on a slope-vertical wall. Slope angle = 30°. Leading edge angle = 45°. Flow velocity = 20 m/s. Kinematic viscosity = 0.5 m²/s. Friction coefficient = 0.5.

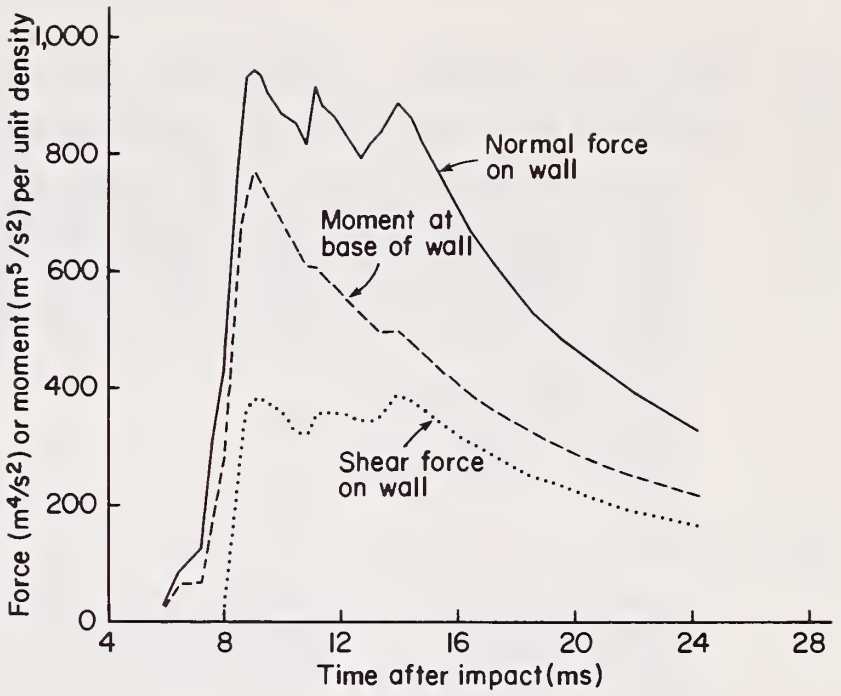

Figure A-8.—Force and moment components as functions of time after impact on a slope-vertical wall. Slope angle = 30°. Leading edge angle = 60°. Flow velocity = 20 m/s. Kinematic viscosity = 0.5 m²/s. Friction coefficient = 0.5.

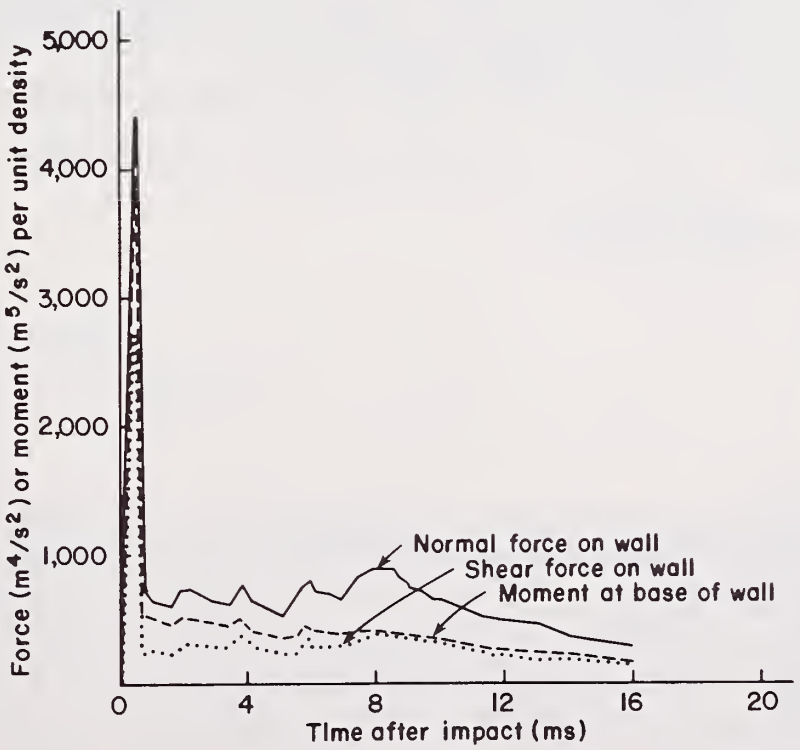

Figure A-9.—Force and moment components as functions of time after impact on a slope-vertical wall. Slope angle = 30°. Leading edge angle = 75°. Flow velocity = 20 m/s. Kinematic viscosity = 0.5 m²/s. Friction coefficient = 0.5.

Appendix B

Listing of Computer Code for Vertical Wall and Inserted Slope-Normal Wall

```
C  PROGRAM IMPACT - VERTICAL WALL.                    <-- SLOPE NORMAL WALL
C
C   EQUIVALENT HORIZONTAL GRID OPTION
C
C      THIS PROGRAM HAS BEEN DEVELOPED TO NUMERICALLY SOLVE (USING
C      FINITE DIFFERENCE TECHNIQUES) THE NAVIER - STOKES EQUATIONS
C      FOR TRANSIENT FLUID FLOW PROBLEMS.  IT WILL BE USED TO SIMULATE
C      THE PROBLEM OF SNOW AND ICE AVALANCHES ON SLOPES OF VARYING SLOPE.
       DIMENSION U(30,30),V(30,30),UN(30,30),VN(30,30),P(30,30),
      1XPUT( 8),H( 30),HN( 30),JT( 30),NAME(20),GX( 30),GY( 30),FRC( 30)
       REAL NU
       INTEGER CYCLE
       READ (105,45) NAME
       WRITE (108,35)
       WRITE (108,45) NAME
C
C * * READ AND PRINT INITIAL INPUT DATA
C
       READ(105,25) (XPUT(I),I=1,8)
       IBAR=XPUT(1) ; JBAR=XPUT(2) ; DELX=XPUT(3) ; DELY=XPUT(4)
       NU=XPUT(5)   ;  FRK=XPUT(6)  ;  TWFIN=XPUT(7)  ;  CWPRT=XPUT(8)
       WRITE (108,50) (XPUT(I),I=1,8)
    25 FORMAT(8F10.0)
    35 FORMAT(1H1)
    45 FORMAT(20A4)
    47 FORMAT(6X,'I',7X,'J',8X,'U',13X,'V',13X,'P',13X,'H',9X,'SUR CELL')
    48 FORMAT(4X,I3,5X,I3,4(4X,1PE10.3),6X,I2)
    49 FORMAT(1X,'CYCL=',I3,1X,'ITR=',I3,1X,'TME=',1PE9.2,1X,'SNH=',E9.2,1X,'UM='
      1E9.2,1X,'FX=',E9.2,1X,'FY=',E9.2,1X,'TB=',E9.2,1X,'PM=',E9.2)
    50 FORMAT(1H ,1X,'IBAR=',F4.0,2X,'JBAR=',F3.0,2X,'DELX=',F6.2,2X,'DELY=',F5.2
      1,2X,'NU=',F4.2,2X,'FRK=',F4.2,2X,'TWFIN=',F5.0,2X,'CWPRT=',F5.0)
    60 FORMAT(8F10.0)
    61 FORMAT(8F10.3)
    70 FORMAT(1H0,35X,'FLOW HEIGHT')
    71 FORMAT(1H0,25X,'ELEVATION CHANGE FOR EACH CELL')
    72 FORMAT(1H0,25X,'BOUNDARY FRICTION COEFFICIENTS')
    73 FORMAT(1H0,25X,'SLOPE-PARALLEL GRAVITY COMPONENT')
    74 FORMAT(1H0,25X,'SLOPE-NORMAL GRAVITY COMPONENT')
    75 FORMAT(1H0,30X,'END OF INPUT DATA'//)
    82 FORMAT(5X,'PROBLEM RUNNING TIME EXCEEDED-CALCULATIONS TERMINATED')
C
C * * COMPUTE CONSTANT TERMS AND INITIALIZE NECESSARY VARIABLES
C
       IMAX=IBAR+2 ; JMAX=JBAR+2
       IM1=IMAX-1  ; JM1=JMAX-1
       RDX=1.0/DELX
       RDY=1.0/DELY
       DELM=DELY/100.
       DELT=.0005
       IM2=IMAX-2
       JM2=JMAX-2
       T=FLG=0.0
       CYCLE=ITER=IND=0
       G=9.8 ; OMG=1.7 ; EPSI=0.5  ; ALPHA=0.1 ; GAMMA=0.1 ; DZRO=1.0
       BETA= OMG/(2.*DELT*(RDX**2+RDY**2))
       ICPRT=INT(CWPRT)
       IF(ICPRT.EQ.1) ICPRT=2
       DO 100 I=1,IMAX
       H(I)=HN(I)=JT(I)=GX(I)=GY(I)=FRC(I)=0.0
       DO 100 J=1,JMAX
  100  U(I,J)=V(I,J)=UN(I,J)=VN(I,J)=P(I,J)=0.0
C
C * * SPECIAL INPUT DATA
C
       READ(105,60)(H(I),I=2,IM1)
       READ(105,60)(HN(I),I=2,IM1)
       IF(FRK.GT.0.0) GO TO 120
```

```
      READ(105,60) (FRC(I),I=2,IM1)
      GO TO 130
  120 DO 125 I=2,IM1
  125 FRC(I)=FRK
  130 CONTINUE
      DO 150 I=2,IM1
      SP=HN(I)/DELX
      CP=SQRT(1.0-SP*SP)
      GX(I)=G*SP
  150 GY(I)=-G*CP
      WRITE(108,70)
      WRITE(108,61)(H(I),I=2,IM1)
      WRITE(108,71)
      WRITE(108,61)(HN(I),I=2,IM1)
      WRITE(108,72)
      WRITE(108,61) (FRC(I),I=2,IM1)
      WRITE(108,73)
      WRITE(108,61)(GX(I),I=2,IM1)
      WRITE(108,74)
      WRITE(108,61)(GY(I),I=2,IM1)
      WRTTE(108,75)
*
C   DETERMINE INITIAL TOP SURFACE INDICES.
*
      DO 240 I=2,IM1
      JT(I)=INT(H(I)*RDY+1.E-6)+2
      IF(JT(I).GT.JM1) JT(I)=JM1
  240 HN(I)=0.0
      H(1)= H(2)
      H(IMAX)= H(IM1)
      JT(1)= JT(2)
      JT(IMAX)= JT(IM1)
*
C * * CALCULATE HYDROSTATIC PRESSURE
*
      DO 280 I=2,IM1
      JT1=JT(I)
      DO 280 J=2,JT1
  280 P(I,J)=-GY(I)*(H(I)-(FLOAT(J)-1.5)*DELY)
*
C * * SET INITIAL VELOCITY
*
      DO 310 I=2,21
      DO 310 J=2,JT(I)
      U(I,J)=20.
  310 V(I,J)=0.0
      ASSIGN 4280 TO KRET
      GO TO 2000
*
C * * START CYCLE
*
 1000 CONTINUE
      ITER=0
      FLG=1.
      ASSIGN 3000 TO KRET
*
C * * COMPUTE TEMPORARY U AND V
*
      DO 1100 I=2,IM1
      JT1=JT(I)
      DO 1100 J=2,JT1
      FUX=((UN(I,J)+UN(I+1,J))*(UN(I,J)+UN(I+1,J))+ALPHA*ABS(UN(I,J)+UN(
     1I+1,J))*(UN(I,J)-UN(I+1,J))-(UN(I-1,J)+UN(I,J))*(UN(I-1,J)+UN(I,J)
     2)-ALPHA*ABS(UN(I-1,J)+UN(I,J))*(UN(I-1,J)-UN(I,J)))/(4.*DELX)
      FUY=((VN(I,J)+VN(I+1,J))*(UN(I,J)+UN(I,J+1))
     1+ALPHA*ABS(VN(I,J)+VN(I+1,J))*(UN(I,J)-UN(I,J+1))
     2-(VN(I,J-1)+VN(I+1,J-1))*(UN(I,J-1)+UN(I,J))
     3-ALPHA*ABS(VN(I,J-1)+VN(I+1,J-1))*(UN(I,J-1)-UN(I,J)))/(4.*DELY)
      FVX=((UN(I,J)+UN(I,J+1))*(VN(I,J)+VN(I+1,J))+ALPHA*ABS(UN(I,J)+UN(
     1I,J+1))*(VN(I,J)-VN(I+1,J))-(UN(I-1,J)+UN(I-1,J+1))*(VN(I-1,J)+VN(
     2I,J))-ALPHA*ABS(UN(I-1,J)+UN(I-1,J+1))*(VN(I-1,J)-VN(I,J)))/(4.*DE
     3LX)
      FVY=((VN(I,J)+VN(I,J+1))*(VN(I,J)+VN(I,J+1))+ALPHA*ABS(VN(I,J)+VN
     1(I,J+1))*(VN(I,J)-VN(I,J+1))-(VN(I,J-1)+VN(I,J))*(VN(I,J-1)+VN(I,J
```

```
     2))-ALPHA*ABS(VN(I,J-1)+VN(I,J))*(VN(I,J-1)-VN(I,J)))/(4.*DELY)
      VISX= NU*((UN(I+1,J)-2.*UN(I,J)+UN(I-1,J))/DELX**2+
     1          (UN(I,J+1)-2.*UN(I,J)+UN(I,J-1))/DELY**2)
      VISY= NU*((VN(I+1,J)-2.*VN(I,J)+VN(I-1,J))/DELX**2+
     1          (VN(I,J+1)-2.*VN(I,J)+VN(I,J-1))/DELY**2)
      U(I,J)= UN(I,J)+DELT*((P(I,J)-P(I+1,J))*RDX + GX(I)-FUX-FUY+VISX)
 1100 V(I,J)= VN(I,J)+DELT*((P(I,J)-P(I,J+1))*RDY + GY(I)-FVX-FVY+VISY)
*
C * * SET BOUNDARY CONDITIONS
*
 2000 CONTINUE
      HN(1)= HN(2)
      HN(IMAX)=HN(IM1)
      JT(1)=JT(2)
      JT(IMAX)=JT(IM1)
C     LEFT WALL CONTINUOUS INFLOW.
C    RIGHT WALL CONTINUOUS OUTFLOW.
      IF(ITER.GT.0) GO TO 2200
      DO 2200 J=1,JMAX
      U(1,J)=U(2,J)
      V(1,J)=V(2,J)
      U(IM1,J)=U(IM2,J)
      V(IMAX,J)=V(IM1,J)
 2200 CONTINUE
C    TOP WALL CONTINUOUS OUTFLOW.
C    BOTTOM WALL RIGID - WITH FRICTION
      DO 2500 I=1,IMAX
      IF(ITER.GT.0) GO TO 2400
      V(I,JM1)=V(I,JM2)
      U(I,JMAX)=U(I,JM1)
 2400 V(I,1)=0.0
 2500 U(I,1)=U(I,2)*(1.0-2.0*FRC(I))
*
C * * FREE SURFACE BOUNDARY CONDITIONS
*
      DO 2650 I=2,IM1
      JT1=JT(I)
      IF(JT(I+1).LT.JT(I)) U(I,JT1)=U(I,JT1-1)
      V(I,JT1)= V(I,JT1-1)-DELY*RDX*(U(I,JT1)-U(I-1,JT1))
 2650 U(I,JT1+1)= U(I,JT1)
*
C * * SPECIAL BOUNDARY CONDITIONS
*
      JNX=1
      J=2
      I=24
 2900 IF(JNX.EQ.6) JNX=1 ; I=I-1
      IF(JNX.EQ.5) I=I-1
      IF(JNX.EQ.3) I=I-1
      IF(J.EQ.21) GO TO 2920
      DO 2910 N=I,IM1
      U(N,J)=0.0
 2910 V(N+1,J)=0.0
      J=J+1
      JNX=JNX+1
      GO TO 2900
 2920 CONTINUE
      GO TO KRET,(3000,4280)
 3000 CONTINUE
*
C * * HAS CONVERGENCE BEEN REACHED
*
      IF(FLG.EQ.0.) GO TO 4000
      ITER=ITER+1
      IF(ITER.LT.500) GO TO 3050
      IF(CYCLE.LT.10) GO TO 4000
      T=1.E+10
      GO TO 4000
 3050 FLG=0.0
*
C * * COMPUTE UPDATED CELL PRESSURE AND VELOCITIES
*
      JB1=2
      DO 3500 I=2,IM1
```

```
      DO 2900 I=24,IM1
      DO 2900 J=1,JM1
      U(I,J)=U0
 2900 V(I+1,J)=0.0
```

```
      JT1=JT(I)
      DO 3500 J=2,JT1
      IF(J.EQ.JT1) GO TO 3100
      GO TO 3200
 3100 ETA=DELY/(HN(I)-(FLOAT(JT1)-2.5)*DELY)
      DELP=(1.0-ETA)*P(I,JT1-1)-P(I,JT1)
      GO TO 3300
 3200 D=RDX*(U(I,J)-U(I-1,J))+RDY*(V(I,J)-V(I,J-1))
      IF(ABS(D/DZRO).GE.EPSI) FLG=1.0
      DELP= -BETA*D
 3300 P(I,J)=P(I,J)+DELP
      U(I,J)=U(I,J)+DELT*RDX*DELP
      U(I-1,J)=U(I-1,J)-DELT*RDX*DELP
      V(I,J)=V(I,J)+DELT*RDY*DELP
 3500 V(I,J-1)=V(I,J-1)-DELT*RDY*DELP
      GO TO 2000
 4000 CONTINUE
*
C * * COMPUTE NEW POSITION FOR TOP SURFACE
*
      DO 4100 I=2,IM1
      JT1=JT(I)
      HV= RDY*(HN(I)-FLOAT(JT1-2)*DELY)
      UAV= 0.5*(U(I-1,JT1) + U(I,JT1))
      H(I)=HN(I)                +DELT*(HV*V(I,JT1)+(1.0-HV)*V(I,JT
     1-1)-0.5*RDX*(UAV*HN(I+1)+GAMMA*ABS(UAV)*(HN(I)-HN(I+1))
     2    -UAV*HN(I-1)-GAMMA*ABS(UAV)*(HN(I-1)-HN(I))))
 4100 CONTINUE
*
C * * CALCULATE CELL IN WHICH SURFACE IS LOCATED AND UPDATE ARRAY
*
      DO 4250 I=2,IM1
      JT(I)=INT(H(I)*RDY+1.0E-6)+2
      IF(JT(I).GT.JM1) JT(I)=JM1
 4250 CONTINUE
      ASSIGN 4280 TO KRET
      GO TO 2000
 4280 CONTINUE
*
C * * CALCULATE TOTAL FLUID VOLUME
*
      FVOL=0.0
      DO 4300 I=2,IM1
 4300 FVOL=FVOL+H(I)*DELX
*
C * * ADVANCE U,V,H ARRAYS.
*
 4910 UMAX=VMAX=0.0
      DO 4900 I=1,IMAX
      HN(I)=H(I)
      DO 4900 J=1,JMAX
      UN(I,J)=U(I,J)
 4900 VN(I,J)=V(I,J)
      DO 4950 I=2,IM2
      DO 4950 J=2,JT(I)
      UT=ABS(UN(I,J))
      VT=ABS(VN(I,J))
      IF(UT.GT.UMAX) UMAX=UT
 4950 IF(VT.GT.VMAX) VMAX=VT
```

THESE INSTRUCTIONS REPLACED BY THOSE LISTED ON PAGE 21.

```
*
C * * COMPUTE BASE FORCES AND MOMENT ON WALL
*
      FX=FY=TB=PM=0.0
      JCY=1
      JNX=1
      J=1
      I=24
 4955 J=J+1
      IF(JCY.EQ.5) GO TO 4990
      PA=P(I,J)+2.*NU*U(I-1,J)/DELY
      IF(PA.GT.PM) PM=PA
      IF(P(I,J).GT.0.0.AND.JNX.EQ.1) GO TO 4960
      IF(P(I,J).GT.0.0.AND.JNX.EQ.2) GO TO 4965
      IF(P(I,J).GT.0.0.AND.JNX.EQ.3) GO TO 4960
      IF(P(I,J).GT.0.0.AND.JNX.EQ.4) GO TO 4965
      IF(P(I,J).GT.0.0.AND.JNX.EQ.5) GO TO 4965
      IF(JNX.EQ.1) JNX=2 ; GO TO 4955
      IF(JNX.EQ.2) JNX=3 ; I=I-1 ; GO TO 4955
      IF(JNX.EQ.3) JNX=4 ; GO TO 4955
      IF(JNX.EQ.4) JNX=5 ; I=I-1 ; GO TO 4955
      IF(JNX.EQ.5) JNX=1 ; I=I-1 ; JCY=JCY+1 ; GO TO 4955
 4960 RX=P(I,J)*DELY+2.*NU*U(I-1,J)
      FX=FX+RX
      FY=FY+NU*(U(I-1,J+1)-U(I-1,J-1))/2.-NU*(V(I,J)+V(I,J-1))
      TB=TB+RX*(FLOAT(J)-1.5)*DELY
      JNX=JNX+1
      GO TO 4955
 4965 RX=P(I,J)*DELY+2.*NU*U(I-1,J)
      RY=P(I,J)*DELY+2.*NU*V(I,J-1)
      SX=-NU*(V(I-1,J-1)+V(I-1,J))/2.
      SY=-NU*(U(I-1,J-1)+V(I,J-1))/2.
      FX=FX+RX+SX
      FY=FY+RY+SY
      TB=TB+RX*(FLOAT(J)-1.5)*DELY+SX*(FLOAT(J)-1.)*DELY-RY*(FLOAT(I)-2
     14.5)*DELX
      JNX=JNX+1
      I=I-1
      IF(JNX.EQ.6) JNX=1 ; JCY=JCY+1
      GO TO 4955
 4990 CONTINUE
      SNHT=H(24)
*
C * * LIST VELOCITY, PRESSURE, AND SURFACE POSITION
*
 5000 WRITE(108,49) CYCLE,ITER,I,SNHT,UMAX,FX,FY,TB,PM
      IF(CYCLE.EQ.ICPRT) GO TO 5030
      IF(CYCLE.NE.ICPRT) GO TO 6000
 5030 ICPRT= ICPRT + INT(CWPRT)
 5060 CONTINUE
      WRITE(108,47)
      DO 5250 I=15,25
      JT1= JT(I)
      JT2=JT1+1
      DO 5250 J=1,JT2
      WRITE(108,48) I,J,U(I,J),V(I,J),P(I,J),H(I),JT1
 5250 CONTINUE
      IF(IND.EQ.2) GO TO 6520
*
C * * RECOMPUTE CONTROL PARAMETERS.
*
 6000 IF(CYCLE.EQ.0) GO TO 6300
      DTX=DELX/UMAX
      DTY=DELY/VMAX
      DELT=AMIN1(DTX,DTY)/3.0
      IF(ITER.LT.10) DELT=1.5*DELT
      IF(NU-1.E-6.LT.0.0) GO TO 6300
      DET=(DELX*DELY)**2/(2.*NU*(DELX**2+DELY**2))
      IF(DELT.LT.DET) GO TO 6300
```

```
      DELT=0.9*DET
 6300 T=T+DELT
      IF(CYCLE.EQ.0) GO TO 6400
      DAX=UMAX*DELT/DELX
      DAY=VMAX*DELT/DELY
      ALPHA=1.35*AMAX1(DAX,DAY)
      IF(ALPHA.GT.1.0) ALPHA=0.95
      GAMMA=ALPHA
      BETA=OMG/(2.*DELT*(RDX**2+RDY**2))
*
C * * TEST FOR PROGRAM TERMINATION.
*
 6400 IF(T.GT.TWFIN) IND=2
      IF(IND.GT.1) GO TO 6500
 6440 CYCLE=CYCLE+1
      GO TO 1000
 6500 T=T-DELT
      GO TO 5060
 6520 WRITE(108,82)
 6600 STOP
      END
```

THESE INSTRUCTIONS FOR THE SLOPE-NORMAL WALL REPLACE BOXED INSTRUCTIONS ON PAGE 20.

```
      IF(H(24).GT.DELM) GO TO 4960
      FX=FY=TB=PM=0.0
      GO TO 4990
 4960 JU=INT(H(24)*RDY+1.E-6)+2
      J=2
      FX=FY=TB=PM=0.0
 4970 IF(J.EQ.JU) GO TO 4980
      RX=P(24,J)*DELY-2.0*NU*(U(24,J)-U(23,J))
      FX=FX-RX
      FY=FY+NU*(U(23,J+1)-U(23,J-1))/2.0-NU*(V(24,J)+V(24,J-1))
      TB=TB+RX*(FLOAT(J)-1.5)*DELY
      J=J+1
      GO TO 4970
 4980 HH=H(24)-DELY*FLOAT(J-2)
      RX=(P(24,J)-2.*NU*(U(24,J)-U(23,J))/DELX)*HH
      FX=FX-RX
      FY=FY+NU*((U(23,J)-U(23,J-1))/DELY-2.*V(24,J-1)/DELX)*HH
      TB=TB+RX*(H(24)-HH/2.0)
      DO 4985 I=2,JU
      PA=P(24,I)+2.0*NU*U(23,I)/DELY
 4985 IF(PA.GT.PM) PM=PA
 4990 CONTINUE
```

Lang, T. E., and R. L. Brown. 1980. Numerical simulation of snow avalanche impact on structures. USDA Forest Service Research Paper RM-216, 21 p. Rocky Mountain Forest and Range Experiment Station, Fort Collins, Colo.

A computer model to predict snow avalanche impact on rigid wall structures is developed based on hydrodynamic equations for viscous flow, and admitting a frictional slip-plane lower boundary. Slope normal and vertical wall configurations which extend higher than the height of avalanche flow are evaluated for normal and shear force and overturning moment from avalanche impact. Impact forces and moment time depend upon avalanche leading edge shape.

Keywords: avalanche, fluid mechanics, impact, forces, pressure, viscosity, avalanche dynamics

Lang, T. E., and R. L. Brown. 1980. Numerical simulation of snow avalanche impact on structures. USDA Forest Service Research Paper RM-216, 21 p. Rocky Mountain Forest and Range Experiment Station, Fort Collins, Colo.

A computer model to predict snow avalanche impact on rigid wall structures is developed based on hydrodynamic equations for viscous flow, and admitting a frictional slip-plane lower boundary. Slope normal and vertical wall configurations which extend higher than the height of avalanche flow are evaluated for normal and shear force and overturning moment from avalanche impact. Impact forces and moment time depend upon avalanche leading edge shape.

Keywords: avalanche, fluid mechanics, impact, forces, pressure, viscosity, avalanche dynamics

Lang, T. E., and R. L. Brown. 1980. Numerical simulation of snow avalanche impact on structures. USDA Forest Service Research Paper RM-216, 21 p. Rocky Mountain Forest and Range Experiment Station, Fort Collins, Colo.

A computer model to predict snow avalanche impact on rigid wall structures is developed based on hydrodynamic equations for viscous flow, and admitting a frictional slip-plane lower boundary. Slope normal and vertical wall configurations which extend higher than the height of avalanche flow are evaluated for normal and shear force and overturning moment from avalanche impact. Impact forces and moment time depend upon avalanche leading edge shape.

Keywords: avalanche, fluid mechanics, impact, forces, pressure, viscosity, avalanche dynamics

Lang, T. E., and R. L. Brown. 1980. Numerical simulation of snow avalanche impact on structures. USDA Forest Service Research Paper RM-216, 21 p. Rocky Mountain Forest and Range Experiment Station, Fort Collins, Colo.

A computer model to predict snow avalanche impact on rigid wall structures is developed based on hydrodynamic equations for viscous flow, and admitting a frictional slip-plane lower boundary. Slope normal and vertical wall configurations which extend higher than the height of avalanche flow are evaluated for normal and shear force and overturning moment from avalanche impact. Impact forces and moment time depend upon avalanche leading edge shape.

Keywords: avalanche, fluid mechanics, impact, forces, pressure, viscosity, avalanche dynamics

Rocky Mountains

Southwest

Great Plains

U.S. Department of Agriculture
Forest Service

Rocky Mountain Forest and Range Experiment Station

The Rocky Mountain Station is one of eight regional experiment stations, plus the Forest Products Laboratory and the Washington Office Staff, that make up the Forest Service research organization.

RESEARCH FOCUS

Research programs at the Rocky Mountain Station are coordinated with area universities and with other institutions. Many studies are conducted on a cooperative basis to accelerate solutions to problems involving range, water, wildlife and fish habitat, human and community development, timber, recreation, protection, and multiresource evaluation.

RESEARCH LOCATIONS

Research Work Units of the Rocky Mountain Station are operated in cooperation with universities in the following cities:

Albuquerque, New Mexico
Bottineau, North Dakota
Flagstaff, Arizona
Fort Collins, Colorado*
Laramie, Wyoming
Lincoln, Nebraska
Lubbock, Texas
Rapid City, South Dakota
Tempe, Arizona

*Station Headquarters: 240 W. Prospect St., Fort Collins, CO 80526